Cell Reports

Report

Differential Stoichiometry among Core Ribosomal Proteins

Graphical Abstract

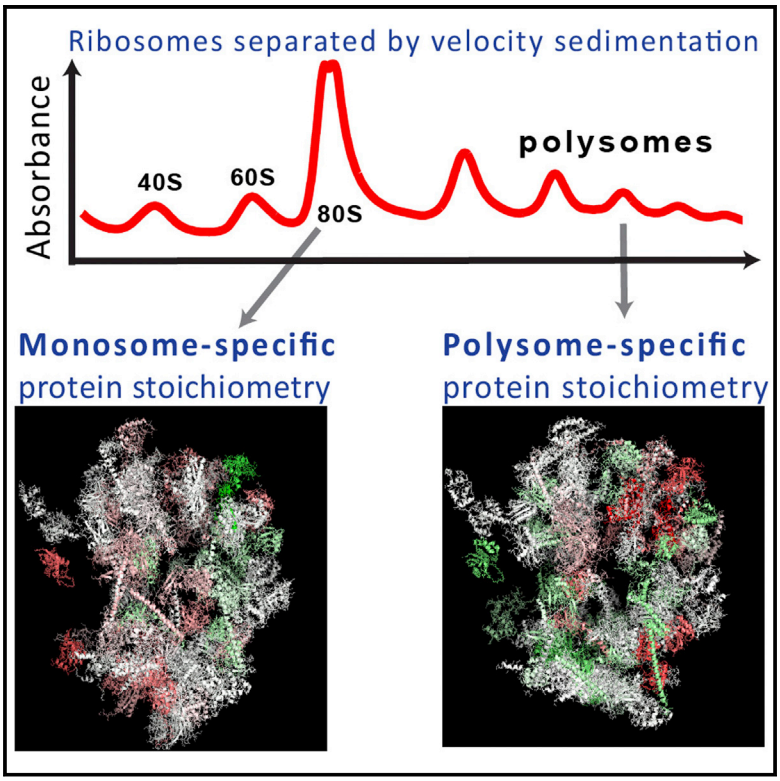

Authors

Nikolai Slavov, Stefan Semrau, Edoardo Airoldi, Bogdan Budnik, Alexander van Oudenaarden

Correspondence

nslavov@alum.mit.edu

In Brief

Indirect evidence gathered over decades has suggested the existence of ribosomes with distinct protein composition and translational specificity in unperturbed wild-type cells. Slavov and colleagues report direct evidence for such ribosome heterogeneity in yeast and mouse stem cells and correlative evidence for its physiological impact on cell growth.

Highlights

- Wild-type yeast and mouse cells build ribosomes with different protein composition
- The stoichiometry among ribosomal proteins (RP) correlates to growth rate
- RP stoichiometry depends on the number of ribosomes bound per mRNA
- RP stoichiometry depends on the growth conditions

Accession Numbers

PXD002816

Slavov et al., 2015, Cell Reports *13*, 1–9
November 3, 2015 ©2015 The Authors
http://dx.doi.org/10.1016/j.celrep.2015.09.056

CellPress

Please cite this article in press as: Slavov et al., Differential Stoichiometry among Core Ribosomal Proteins, Cell Reports (2015), http://dx.doi.org/10.1016/j.celrep.2015.09.056

Cell Reports
Report

Differential Stoichiometry among Core Ribosomal Proteins

Nikolai Slavov,[1,2,*] Stefan Semrau,[3] Edoardo Airoldi,[2] Bogdan Budnik,[2] and Alexander van Oudenaarden[4]
[1]Department of Bioengineering, Northeastern University, Boston, MA 02115, USA
[2]Department of Statistics and FAS Center for Systems Biology, Harvard University, Cambridge, MA 02138, USA
[3]Leiden Institute of Physics, Leiden University, 2333 CC Leiden, the Netherlands
[4]Hubrecht Institute, Royal Netherlands Academy of Arts and Sciences and University Medical Center Utrecht, Uppsalalaan 8, 3584 CT Utrecht, the Netherlands
*Correspondence: nslavov@alum.mit.edu
http://dx.doi.org/10.1016/j.celrep.2015.09.056

SUMMARY

Understanding the regulation and structure of ribosomes is essential to understanding protein synthesis and its dysregulation in disease. While ribosomes are believed to have a fixed stoichiometry among their core ribosomal proteins (RPs), some experiments suggest a more variable composition. Testing such variability requires direct and precise quantification of RPs. We used mass spectrometry to directly quantify RPs across monosomes and polysomes of mouse embryonic stem cells (ESC) and budding yeast. Our data show that the stoichiometry among core RPs in wild-type yeast cells and ESC depends both on the growth conditions and on the number of ribosomes bound per mRNA. Furthermore, we find that the fitness of cells with a deleted RP-gene is inversely proportional to the enrichment of the corresponding RP in polysomes. Together, our findings support the existence of ribosomes with distinct protein composition and physiological function.

INTRODUCTION

Ribosomes catalyze protein synthesis but have only a few characterized roles in regulating it (Mauro and Edelman, 2002; Xue and Barna, 2012). Rather, the most-studied molecular regulatory mechanisms of translation are mediated by eukaryotic initiation factors, RNA binding proteins, and microRNAs (Hendrickson et al., 2009; Fabian and Sonenberg, 2012). The characterized catalytic role of the ribosomes corresponds well to the model of the ribosome as a single complex with a fixed stoichiometry: four ribosomal RNAs and 80 core RPs (Warner, 1999; Ben-Shem et al., 2011), some of which are represented by several paralogous RPs. Despite the longstanding interest in ribosome structure and function, the exact stoichiometry and possible heterogeneity of the ribosomes have been challenging to measure directly (Weber, 1972; Westermann et al., 1976; Hardy, 1975). Such measurements are enabled by modern quantitative mass spectrometry (MS). Indeed, MS has transformed our understanding of protein complexes, such as proteasomes (Wang et al., 2007) and nuclear pore complexes (Ori et al., 2013), by demonstrating variability among their protein subunits. Furthermore, quantitative MS has proved useful in characterizing ribosome biogenesis (Chen and Williamson, 2013).

Studies of eukaryotic ribosomes (Mazumder et al., 2003; Galkin et al., 2007; Komili et al., 2007; Kondrashov et al., 2011; Horos et al., 2012; Lee et al., 2013) have demonstrated that (1) genetic perturbations to the core RPs specifically affect the translation of some mRNAs but not others and (2) mRNAs coding for core RPs are transcribed, spliced, and translated differentially across physiological conditions (Ramagopal and Ennis, 1981; Ramagopal, 1990; Parenteau et al., 2011; Slavov and Dawson, 2009; Slavov and Botstein, 2011, 2013; O'Leary et al., 2013; Slavov et al., 2014; Gupta and Warner, 2014; Jovanovic et al., 2015). These results suggest the hypothesis (Mauro and Edelman, 2002; Gilbert, 2011; Xue and Barna, 2012) that, depending on the tissue type and the physiological conditions, cells can alter the stoichiometry among the core RPs comprising the ribosomes and thus, in turn, alter the translational efficiency of distinct mRNAs. Alternatively, differential RP-expression can reflect extra ribosomal functions of the RPs (Mazumder et al., 2003; Wool, 1996; Warner and McIntosh, 2009). Furthermore, polysomes (multiple ribosomes per mRNA) from different cancer cell lines have similar core RP stoichiometries (Reschke et al., 2013). Thus, the variable RP stoichiometry in the ribosomes of wild-type cells that is suggested by the ribosome specialization hypothesis remains unproven.

We sought to test whether wild-type cells have ribosomes with differential RP stoichiometry. For this test, we chose two divergent eukaryotes: budding yeast *Saccharomyces cerevisiae* and mouse ESC. We chose budding yeast because of our previous observations that RPs are differentially transcribed across growth rates (Slavov and Botstein, 2011, 2013) and that RP levels change differentially between glucose and ethanol carbon source (Slavov et al., 2014). To investigate whether such differential transcription of RPs affects the ribosomal composition, we used the same media as in our previous experiments, minimal media supplemented with 0.2% glucose. In this media, unlike in rich media supplemented with 2% glucose, yeast cells have a prominent monosomal peak that may reflect different translational regulation (Ashe

Please cite this article in press as: Slavov et al., Differential Stoichiometry among Core Ribosomal Proteins, Cell Reports (2015), http://dx.doi.org/10.1016/j.celrep.2015.09.056

et al., 2000; Castelli et al., 2011; Vaidyanathan et al., 2014). We chose embryonic stem cells to test differential RP stoichiometry in wild-type mammalian cells because of the interesting phenotypes of RP deletions/knockdowns in ESC. For example, haploinsufficiency for Rps5, Rps14, or Rps28 interferes with ESC differentiation but not with their self-renewal (Fortier et al., 2015). Furthermore, unlike heteroploid cancer cell lines grown in culture, ESC have a high monosomes-to-polysomes ratio, consistent with the possibility of differential translational regulation (Sampath et al., 2008; Fortier et al., 2015).

RESULTS

Differential Stoichiometry among Core RPs in Mouse ESC

To explore whether the stoichiometry among core RPs can vary, we first isolated monosomes and polysomes from exponentially growing mouse embryonic stem cells (ESC), doubling every 9 hr, Figure S1A. The ESC ribosomes were isolated by velocity sedimentation in sucrose gradients (Figure 1A); see Experimental Procedures. To confirm that the prominent monosomal peak is reflective of ESC biology and not of poor ribosome fractionation, we also fractionated the ribosomes of neuroprogenitor cells derived from the ESC. Despite growing three times slower (doubling time 29 hr) than the ESC, the neuroprogenitor cells have a larger fraction of their ribosomes in polysomal complexes, Figure S1B. This observation confirms earlier findings by Sampath et al. (2008), and thus further bolsters the conclusion that a low polysome-to-monosomes ratio is characteristic of ESC.

Having isolated monosomes and polysomes, we sought to quantify their protein composition. The proteins from individual sucrose fractions were digested to peptides, labeled with tandem mass tags (TMT), and quantified on Orbitrap Elite based on the MS2 intensities of the TMT reporter ions; see Supplemental Information. The monosomal sample was quantified in two replicates (1a and 1b), and the results indicate very high reproducibility (ρ = 0.92; Figure 1B). To control for protease and peptide biases, the proteins from each analyzed sucrose fraction were digested either by trypsin (T) or by lys-C (L), and peptides from each digestion were quantified independently. Because of the different specificity of trypsin and lys-C, most RP peptides (1,058) were identified and quantified only in the trypsin or only in the lys-C digestion, while only 269 peptides were identified and quantified in both digestions. Thus, only very few peptide-specific biases (such as co-isolation interference) may be shared between the two digestions.

The measured levels of a unique peptide (a peptide present in a single RP) reflect the levels of the corresponding RP, post-translational modifications (PTMs) of the peptide (if any), and measurement error. We quantify on average ten distinct RP peptides per RP (Figure S2A), and the levels of these peptides allow both the estimation of the RP levels and the consistency of these estimates. To depict both the estimates and their consistency, we display the full distributions of relative levels of all peptides unique to an RP as boxplots in Figures 1C and 1D. The RP levels across the sucrose gradient (estimated as the median of the levels of unique peptides) indicate that some RPs are enriched in monosomes (Figure 1C), while other RPs are enriched in polysomes (Figure 1D). Each RP group includes proteins from both the large (60S) and the small (40S) subunits of the ribosomes and thus differential loss of 40S or 60S cannot account for the RP levels displayed in Figures 1C and 1D. Indeed, normalizing for the total amount of 40S and 60S proteins in each fraction does not alter significantly the results. The RP enrichment in Figure 1 is substantially higher than the measurement noise, consistent across replicates and across distinct peptides, and highly statistically significant at false discovery rate (FDR) $<10^{-6}$. The relative levels of all RPs with quantified unique peptides are displayed in Figure 2 to illustrate the global pattern of RP levels across monosomes and polysomes. This pattern shows more RPs whose variability is consistent across replicates and enzymatic digestions. In contrast, the levels of RPs buried in the core of the ribosomes remain constant, with estimates fluctuating within the tight bounds of the measurement noise, Figure 2. This fixed stoichiometry among RPs constituting the ribosomal core suggests that even ribosomes lacking some surface RPs likely have the same core structure.

In principle, if only a few peptides are quantified per RP, the measured peptide variability might reflect reciprocal variability in corresponding PTM isoforms (if any) across the sucrose gradients; e.g., the unmodified isoform is enriched in monosomes and a phosphorylated isoform is enriched in polysomes. Such differential distribution of PTM isoforms (if any) is interesting since it represents another layer of ribosome regulation but cannot explain the data for an RP quantified by dozens of peptides spanning the protein length and indicating highly consistent fold changes across the sucrose gradient; see Figures 1 and S2 and Supplemental Information.

We further tested the differential RP stoichiometry with an independent method, western blots, and in another strain of mouse ESC. Consistent with the MS data in Figure 2, the western blot data (Figure S3) indicate that Rps29 and Rps14 are enriched in polysomes, Rpl11 is enriched in monosomes, and Rpl32 does not change beyond the measurement noise.

Differential Stoichiometry among Core RPs in Yeast

Having found differential stoichiometry among mouse RPs, we sought to further explore (1) whether such ribosome heterogeneity is conserved to budding yeast and (2) whether the RP stoichiometry can change with growth conditions and metabolic state. To this end, we employed sucrose gradients to separate the ribosomes from yeast cells grown in minimal media with either glucose or ethanol as the sole source of carbon and energy (Slavov et al., 2014); see Supplemental Information. Consistent with previous observations that the type and the concentration of the carbon source influence the ratio of monosomes to polysomes (Ashe et al., 2000; Castelli et al., 2011; Vaidyanathan et al., 2014), the ratio of monosomes to polysomes in our yeast cells grown in 0.4% ethanol (Figure 3A) or in 0.2% glucose (Figure 3B) is higher than is typically observed for yeast grown in rich media containing 2% glucose. As in mouse, some RPs are enriched in monosomes (Figure 3C) and others in polysomes (Figures 3D and 3E). This enrichment is reproducible (correlation between replicates ρ = 0.97; Figure 3F) and consistent across independent unique peptides whose levels are shown as boxplot distributions in Figures 3C and 3D.

Please cite this article in press as: Slavov et al., Differential Stoichiometry among Core Ribosomal Proteins, Cell Reports (2015), http://dx.doi.org/10.1016/j.celrep.2015.09.056

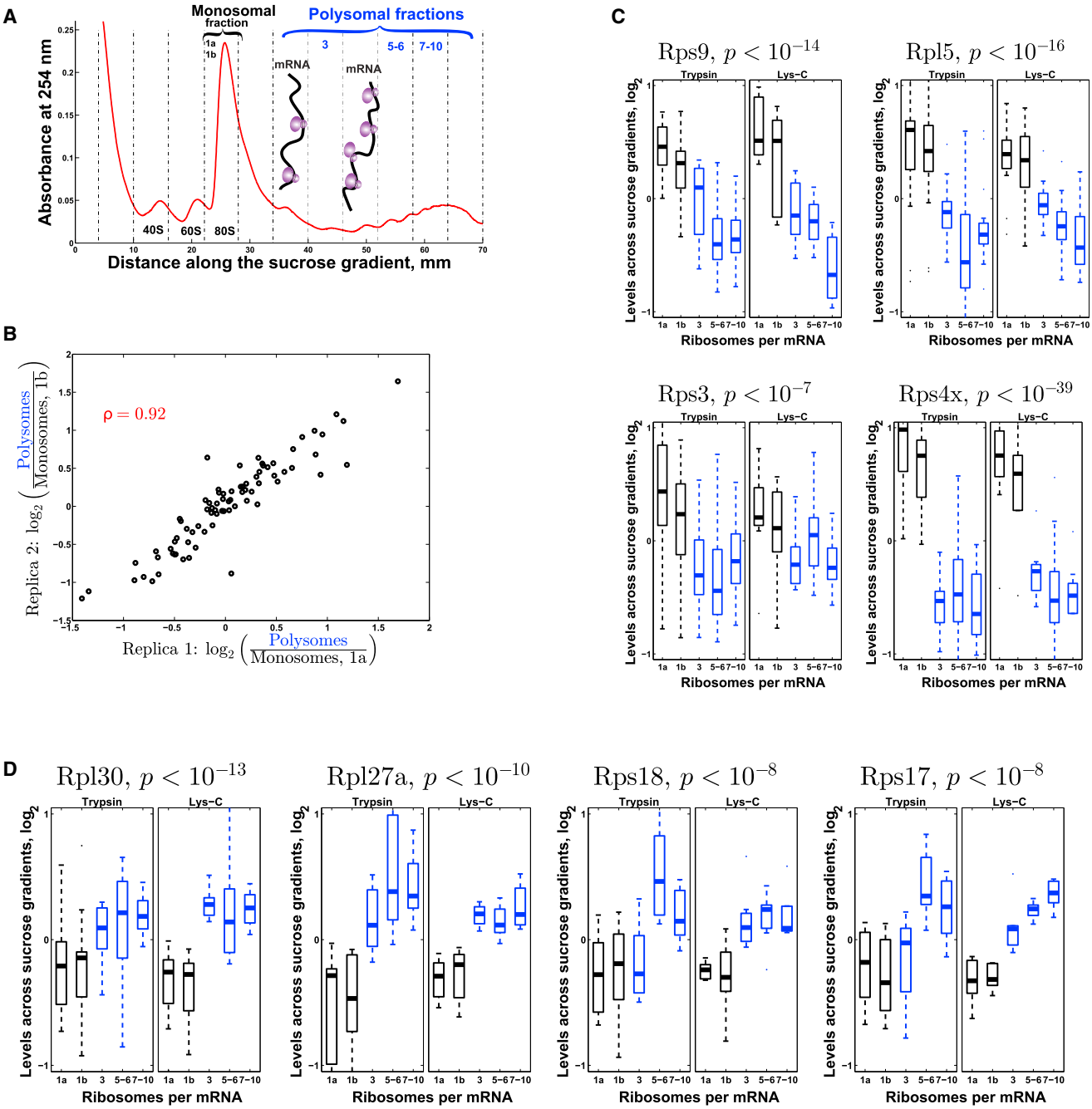

Figure 1. The Stoichiometry among Core RPs in Mouse Ribosomes Depends on the Number of Ribosomes per mRNA

(A) Velocity sedimentation in sucrose gradients allow separating ribosomes that are free or bound to a single mRNA (monosomes, depicted in black) from multiple ribosomes bound to a single mRNA (polysomes, depicted in blue). The absorbance at 254 nm reflects RNA levels, mostly ribosomal RNA. The vertical dashed lines indicate the boundaries of the collected fractions. Fractions are labeled at the top with numbers reflecting the number of ribosomes per mRNA.

(B) Replicates MS measurements of the monosomes (A and B) indicate reproducible estimates for RP enrichment in polysomes.

(C and D) Some RPs are enriched in monosomes (C) and others in polysomes (D). The relative levels of each RP are quantified as the median levels of its unique peptides, and the probability that the RP levels do not change across the quantified fractions is computed from ANOVA (indicated at the top). The distributions of levels of all unique peptides from trypsin (left panels) and from lys-C (right panels) digestions are juxtaposed as boxplots to depict the consistency of the estimates across proteases, different peptides, and experiments.

For each fraction, the mean intensity of all RP peptides was normalized to 1. On each box, the central line is the median, the edges of the box are the 25th and 75th percentiles, and the whiskers extend to the most extreme data points.

See also Figures S1 and S2.

Please cite this article in press as: Slavov et al., Differential Stoichiometry among Core Ribosomal Proteins, Cell Reports (2015), http://dx.doi.org/10.1016/j.celrep.2015.09.056

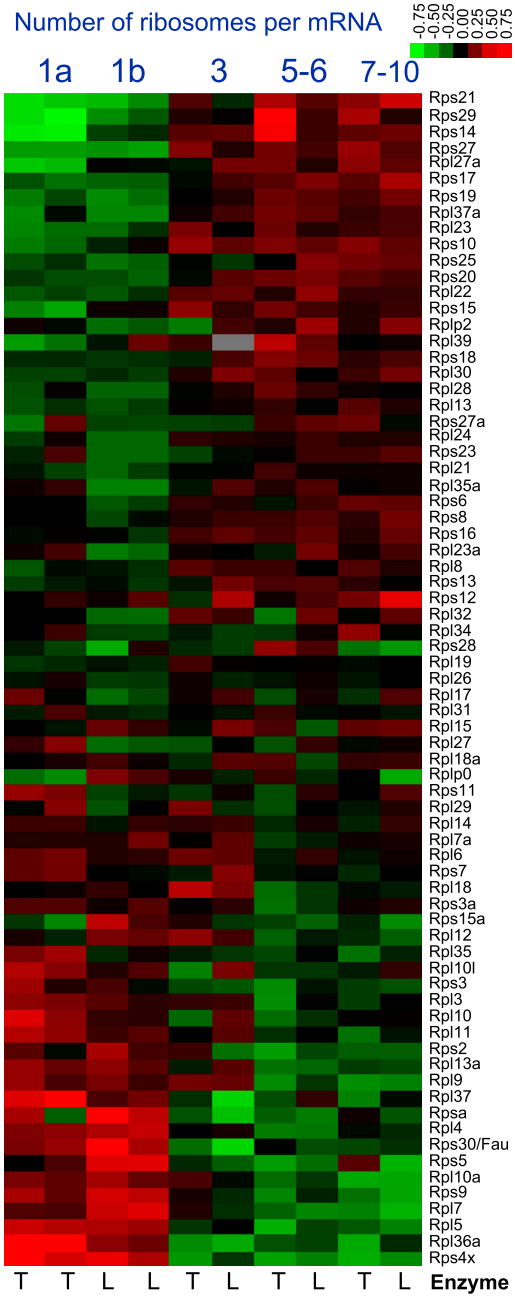

Figure 2. Global Pattern of Differential Stoichiometry among Mouse RPs across Sucrose Gradients

The relative levels of core RPs in monosomes and polysomes were quantified by MS and found to vary depending on the number of ribosomes bound per mRNA. The measurement noise was estimated by (1) replica quantification of the monosomal fraction (by using different tandem mass tags reporter ions, 126 or 131) and by (2) estimating RP levels separately using either trypsin (T) or lys-C (L) digestion, as indicated at the bottom of each column. The $\log_2$ levels of each RP are shown relative to their mean.

See also Figures S2 and S3 and Tables S1, S2, and S3.

We investigated whether the differential levels of RPs, both in yeast and in mouse, may reflect the presence of ribosome biogenesis complexes or other extra-ribosomal complexes containing RPs. We estimated that biogenesis factors are over 200-fold less abundant than RPs across all samples (Figure S4A), and 80-fold less abundant even in the monosomal fractions (Figure S4B) where ribosome biogenesis particles are enriched; see Supplemental Information. These data suggest that the proteins derived from immature ribosomes can contribute about 1%–3% to the RP fold changes, while some measured RP fold changes exceed 100% (Figure 1). The contribution of immature ribosomes to our RP estimates can be further tested by using the order in which RPs are incorporated into the small subunits. This order has been established for bacterial RPs in vitro (Mulder et al., 2010) and confirmed in vivo (Chen and Williamson, 2013). We used this order, as well as the correspondence and nomenclature between orthologous bacterial and mammalian RPs (Jenner et al., 2012), to test the trends that are expected if biogenesis particles are abundant enough to influence RP quantification: RPs that are incorporated early should be enriched in the monosomal fractions and depleted from polysomal fractions; the late RPs should show the converse trend. While these trends are observed for some RPs (such as S4 and S14), the opposite trends are observed for other RPs (such as S3, S5, S11, and S15; Figure S4C). The overall pattern of relative RP levels in Figure 2 cannot be fully accounted for by the order of RP incorporation during ribosome biogenesis (Figure S4C).

The pattern of relative RP levels shown in Figures 3C–3E indicates that RP stoichiometry depends on two factors: the number of ribosomes per mRNA (as in mouse) and the carbon source in the growth media; the RP levels that are higher in glucose compared to ethanol also tend to increase with the number of ribosomes per mRNA (Figures 3C–3E). Furthermore, the ratios between the polysomal and monosomal levels of yeast RPs correlate to the corresponding ratios for their mouse orthologs (Figure 3G; p value <0.03), suggesting that the RP-stoichiometry differences between monosomes and polysomes are conserved across yeast and mouse.

Many yeast RPs are represented by two highly homologous paralogs, and we explored whether the exchange among paralogs (one paralog substituting for the other) can account for the measured differential stoichiometry in Figure 3E. The levels of paralogs localized on the surface of the ribosome, such as Rpl17a and Rpl17b, are positively correlated and thus inconsistent with paralog exchange across the analyzed ribosomes (Figure 3E). In contrast, RPs embedded deep in the core of the ribosomes either remain constant (the estimated fluctuations of their levels are within error bars) or their paralogs exchange (e.g., the levels of Rpl37a and Rpl37b are anticorrelated; see Figure 3E), indicating that each ribosome has a copy of Rpl37. In general, the RPs whose levels differ the most among the different fractions are located on the surface of the yeast ribosomes, as can be seen from their 3D color-coded rendition in File S1 (Movie S1 and PDB files).

RP Enrichment in Polysomes Correlates to Fitness

Next, we tested the differential RPs stoichiometry and its phenotypic consequences by independent fitness measurements. Our

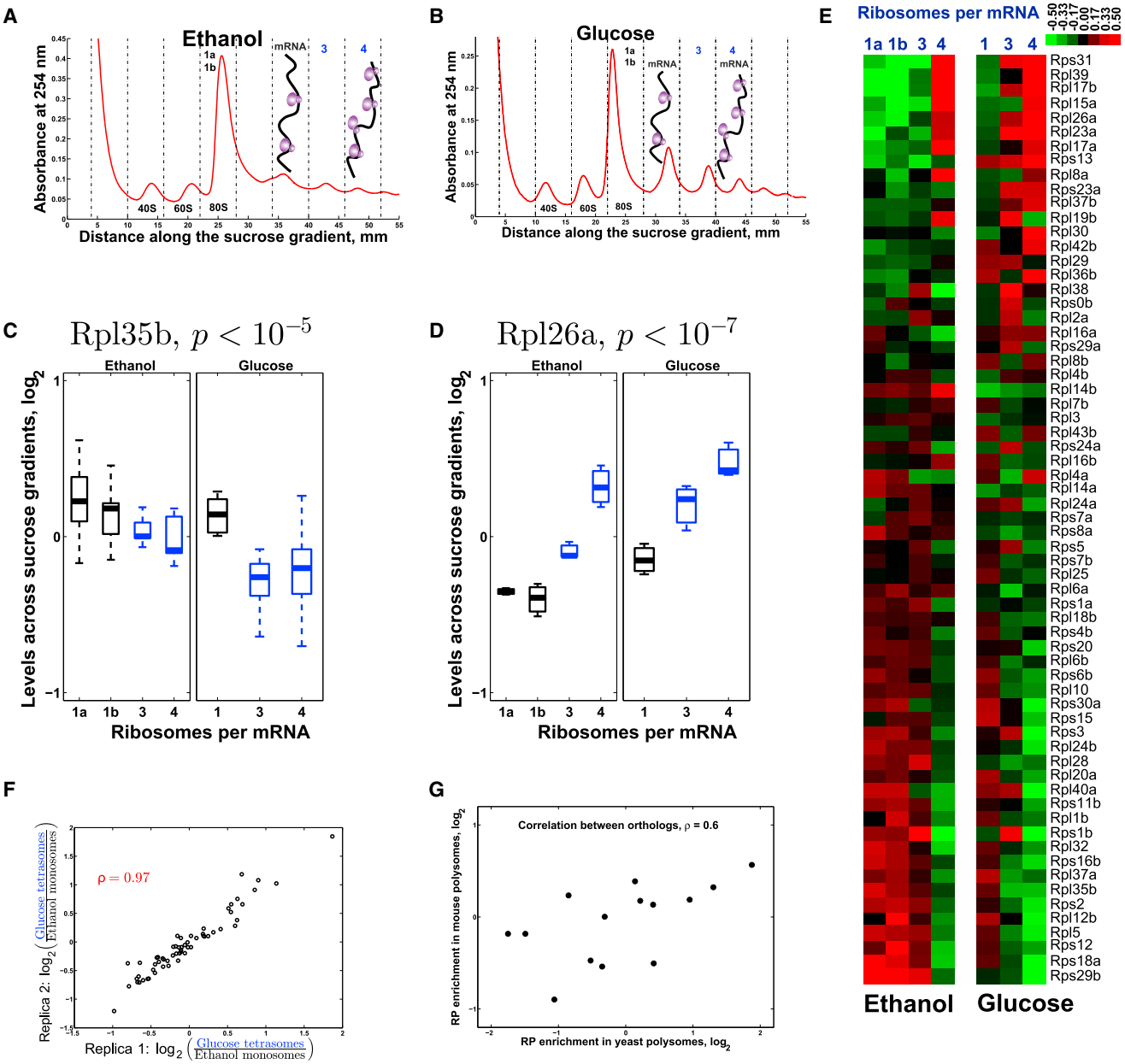

Figure 3. The Stoichiometry among Core RPs in Yeast Ribosomes Depends Both on the Number of Ribosomes per mRNA and on the Physiological Condition

(A and B) Ribosomes from either ethanol (A) or glucose (B) grown yeast were separated by velocity sedimentation in sucrose gradients. Depiction is as in Figure 1A.

(C) Rpl35b is enriched in monosomes ($p < 10^{-3}$) and in ethanol carbon source ($p < 10^{-3}$).

Depiction is as in Figure 1. The p value at the top is computed from ANOVA and quantifies the probability of observing the variability of Rpl35b peptides by chance.

(D) Rpl26a is enriched in polysomes ($p < 10^{-9}$) and in glucose carbon source ($p < 10^{-4}$).

(E) Levels of core RPs in the sucrose fractions estimated from their unique peptides quantified by MS. The RP levels vary depending on the carbon source (glucose or ethanol) and on the number of ribosomes bound per mRNA, indicated at the top. Monosomes from ethanol grown yeast were quantified in two biological replicates (first two columns). The $\log_2$ levels of each RP are shown relative to their mean. See File S1 (Movie S1 and PDB files) for color-coded depiction of these data on the 3D structure of the yeast ribosome.

(F) The RP fold changes between the tetrasomes of yeast grown in glucose carbon source and the monosomes of yeast grown in ethanol carbon source are highly reproducible. The ethanol samples were collected and processed independently and compared to the glucose tetrasomes.

(G) The $\log_2$ ratios between polysomal and monosomal levels of mouse RPs are plotted against the corresponding $\log_2$ ratios of their orthologous yeast RPs. The significant (p value <0.03) positive correlation between these ratios suggests that the differential RP stoichiometry is conserved across yeast and mouse. The plot includes all orthologous RP pairs with over 65% sequence identity between yeast and mouse.

See also Figures S2 and S4 and Tables S4 and S5.

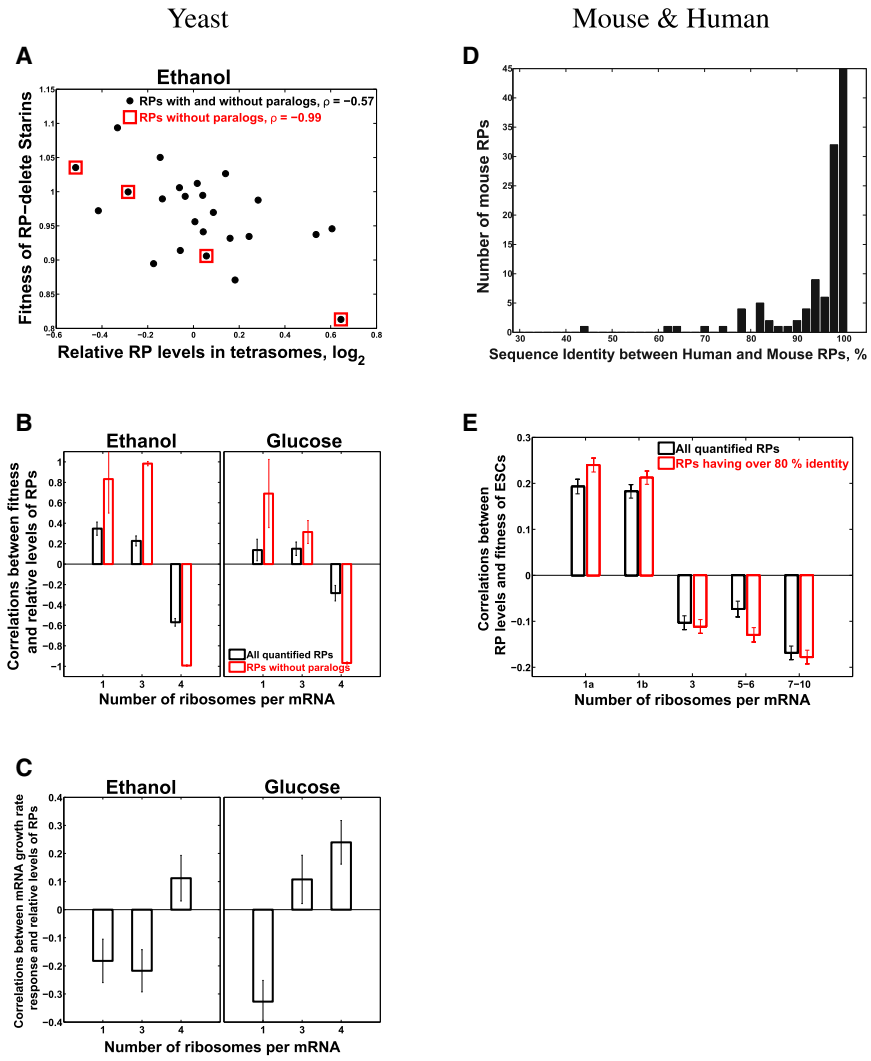

Figure 4. The Relative Levels of RPs across Monosomes and Polysomes Correlate Significantly to the Fitness of Yeast and Mammalian Cells Lacking the Genes Encoding These RPs

(A) The fitness of RP-deleted yeast strains (Qian et al., 2012) is inversely proportional (p value $<4 \times 10^{-3}$) to the relative levels of the corresponding RPs in tetrasomes from yeast growing on ethanol carbon source. The RPs without paralogs are marked with red squares.

(B) Extension of the analysis in (A) to all sucrose fractions: correlations between the relative RP levels from Figure 3E and the fitnesses of strains lacking the corresponding RP genes (Qian et al., 2012). The correlations are shown either for all quantified RPs or only for RPs without paralogs.

(C) Correlations between the relative levels of the RPs from Figure 3E and the their transcriptional growth rate responses (slopes). The growth-rate slopes were previously computed by regressing ($R^2 > 0.87$) the levels of mRNAs in glucose-limited steady-state cultures of yeast against the growth rates of the cultures (Slavov and Botstein, 2011).

(D) Distribution of sequence identity between human RPs and their closest mouse orthologs; the sequences and annotations for RPs are from SWISS-PROT.

(E) Extension of the analysis for yeast in (A) and (B) to mouse: correlations between the relative levels of mouse RPs from Figure 2 and the fitness of human ESC lacking the corresponding human ortholog (Shalem et al., 2014). The correlations are shown either for all quantified RPs or only for RPs whose sequence identity between mouse and human exceeds 80%. The correlation for monosomes is shown in replicates (1a and 1b).

See also Figure S5. All error bars are SD from bootstrapping.

observation that the RP stoichiometry depends on the number of ribosomes bound per mRNA parallels measurements of higher translational activity of polysomes compared to monosomes (Warner et al., 1963; Goodman and Rich, 1963); some studies have even reported that the translational activity per ribosome increases with the number of ribosomes bound per mRNA (Noll et al., 1963; Wettstein et al., 1963), but this finding has not been widely reproduced. We therefore hypothesized that genetic deletions of RPs enriched in the more active ribosomes—as compared to RPs enriched in less active ribosomes—may result in a larger decrease of the translation rate and thus lower fitness. To test this hypothesis, we computed the correlation (Figure 4A) between the fitness of yeast strains with single RP gene deletions (Qian et al., 2012) and the corresponding relative RP levels measured in the tetra-ribosomal fraction (four ribosomes per mRNA). Consistent with our hypothesis, the fitness of strains lacking RP genes is inversely proportional to the relative levels of the corresponding RPs in the tetra-ribosomes (Figure 4A). Extending this correlation analysis to the RP levels in all sucrose fractions shown in Figure 3E results in a correlation pattern (Figure 4B) that further supports our hypothesis by showing the opposite dependence for fractions with fewer ribosomes per mRNA: the fitness of strains lacking RP genes is proportional to the relative levels of the corresponding RPs in fractions with fewer ribosomes per mRNA (Figure 4B). This correlation pattern holds both for ethanol and for glucose carbon sources. To mitigate possible artifacts in the fitness data due to potential chromosome duplications in the deletion strains, we computed the correlations between the RP levels and the fitness of the corresponding RP deletion strains only for RPs without paralogs (thus unlikely to be affected by chromosome duplication) and found much higher magnitudes of the correlations (Figures 4A and 4B). This result suggests that the differential RP stoichiometry is not limited to paralogous RPs substituting for each other.

To further explore the functional significance of the differential RP stoichiometry, we examined whether polysome-enriched RPs are preferentially induced at higher growth rates. We previously found that the degree of growth-rate-dependent transcriptional induction varies significantly across RPs (Brauer et al.,

2008; Slavov and Botstein, 2011, 2013; Slavov et al., 2012). We quantified the growth-rate responses of RPs by regressing their mRNA levels on growth rates and computing growth rate slopes. The magnitudes of RP growth-rate slopes range from positive (mRNA levels increase with increasing growth rate) to negative (mRNA levels decrease with increasing growth rate), see Figure S5. Analogously to our fitness analysis (Figure 4A), we correlated the growth-rate slopes to the relative RP levels from Figure 3E. Consistent with our hypothesis, the correlation pattern (Figure 4C) indicates that the higher the growth-rate slope of a RP, the higher its enrichment in sucrose fractions corresponding to increasing numbers of ribosomes per mRNA.

We extended our fitness analysis from yeast to mouse using the published depletion data from CRISPR knockouts in human ESC (Shalem et al., 2014); see Supplemental Information. We used BLAST to identify the closest mouse orthologs of each human RP with depletion data (Figure 4D) and correlated the fitness of human ESC lacking the human RP orthologs to the RP levels across sucrose fractions that we measured (Figure 2). The correlation pattern (Figure 4E) is similar to the one in yeast (Figures 4A–4C) and highly significant (FDR <0.1%). This pattern indicates that the fitness of ESC lacking RP genes is directly proportional to the relative RP levels in monosomes and inversely proportional to the relative RP levels in polysomes. The magnitude of this inverse proportionality increases with the number of ribosomes per mRNA (Figure 4E), consistent with our hypothesis. The fact that the fitness of human ESC lacking RPs correlates significantly to the levels of the corresponding mouse orthologous RPs suggests that the differential RP stoichiometry and its biological functions are likely conserved across mouse and human. The magnitude of this correlation increases when the correlation is computed based only on the orthologs whose sequences are over 80% identical between mouse and human (Figure 4E), providing further evidence for the conserved fitness consequences of the altered RP stoichiometry.

DISCUSSION

For decades, the ribosome has been considered the preeminent example of a large RNA-protein complex with a fixed stoichiometry among the constituent core RPs (Warner, 1999; Ben-Shem et al., 2011). However, the direct and precise measurements of RP levels required to support this view have been very challenging. Prior to our work, the most direct and precise quantification of RP stoichiometry that we know of is based on measuring the radioactivity from RPs labeled with ^{14}C or ^{3}H and separated on 2D gels. Some of these studies (Weber, 1972; Westermann et al., 1976) achieved very high precision (SE <10%) and reported over 2-fold deviation from 1:1 stoichiometry for multiple RPs. Other studies of prokaryotic ribosomes (Hardy, 1975) achieved lower precision, and the deviation from 1:1 stoichiometry was within the experimental error of the measurements. The results reported in Weber (1972), Westermann et al. (1976), and Hardy (1975) are all consistent with our findings, albeit our measurements are limited to eukaryotic ribosomes. This prior work and our measurements reflect population averages across a heterogeneous pool of ribosomes and thus likely underestimate the magnitude of the variability among RP stoichiometries.

A simple mechanism that may account for our observations is that the rates of translation initiation and elongation depend on the RP composition. Ribosomes whose RP composition corresponds to higher ratios between the initiation and the elongation rates are likely to be found in fractions with multiple ribosomes per mRNA. Conversely, ribosomes whose RP composition corresponds to lower ratios between the initiation and the elongation rates are likely to be found in fractions with fewer ribosomes per mRNA. Indeed, increased growth rate on glucose carbon source that we find associated with altered RP stoichiometry has been previously reported to be associated with faster elongation rates (Bonven and Gulløv, 1979; Young and Bremer, 1976).

Velocity sedimentation in sucrose gradients is unlikely to perfectly separate ribosomes based on their RP composition. For example, short mRNAs and the ribosomes translating them can be found only in the fractions containing few ribosomes per mRNA regardless of the efficiency of translation and the RP composition of the ribosomes (Arava et al., 2003). Similarly, even the most highly translated mRNA that is likely to be translated by polysome-type ribosomes will go through a stage when only a single ribosome is loaded and thus will be found in the monosomal fraction. Other factors may also contribute to the mixing of different ribosomes in each sucrose fraction, including variation in the mRNA length, any degree of ribosome runoff, and mRNA shearing during sample handling, if any. None of these factors, however, is likely to artifactually contribute to the differential RP stoichiometry that we observe. Rather, the presence of ribosomes with different RP compositions in the same sucrose fraction would average out and decrease the differences, resulting in underestimation of the RP variability.

The conserved difference between monosomal and polysomal ribosomes (Figure 3G) raises the question about the activity of monosomes, especially given the lower estimates for their translational activity (Warner et al., 1963; Wettstein et al., 1963). The RP levels in Figure 3E indicate that the RP composition of trisomes in ethanol is more similar to the composition of monosomes than to tetrasomes. This observation shows that monosomes may have similar RP composition to polysomes, suggesting that the RP composition of monosomes is not necessarily indicative of a nonfunctional state.

The correlations between RP composition and fitness can be explained by the expectation that the higher the translational activity of a ribosome, the higher the fitness cost of its perturbation in rapidly growing stem cells. The key factor required for this expectation is the differential RP stoichiometry that we measured. The differential RP stoichiometry in the absence of external perturbations suggests that cells use it as a regulatory mechanism of protein synthesis. One such example might be the preferential transcriptional induction of polysome-enriched RPs at higher growth rates (Figure 4C).

Variable mammalian RPs, such as Rps4x, Rps14, Rps20, Rpl5, Rpl10, and Rpl27, directly bind mRNAs (Castello et al., 2012; Kwon et al., 2013), and this binding might mediate translational regulation as previously suggested (Mauro and Edelman, 2002; Landry et al., 2009; Mazumder et al., 2003). Furthermore, deletions or overexpressions of many of the variable RPs (Figure 1B) have well-characterized phenotypes both in development

and in cancer. For example, the knockdown or haploinsufficiency of the polysomally enriched Rps19 (Figure 1B) causes Diamond Blackfan anemia by selectively affecting the synthesis of some proteins but not of others (Horos et al., 2012). Interestingly, our data indicate that RPs that are frequently mutated in cancers, such as Rpl5 and Rpl10 (De Keersmaecker et al., 2013; Lawrence et al., 2014), are enriched in the monosomes (Figures 1A and 2). Conversely, RPs whose (over)expression promotes cancer, such as Rpl30, Rps20, and Rpl39 (De Bortoli et al., 2006; Dave et al., 2014), are enriched in the polysomes (Figures 1B and 2). One interpretation, among others, of these data is that loss of function of monosomally enriched RPs or overexpression of polysomally enriched RPs might promote protein synthesis and cancer cell growth.

EXPERIMENTAL PROCEDURES

All yeast experiments used a prototrophic diploid strain (DBY12007) with a S288c background and wild-type HAP1 alleles (Slavov and Botstein, 2011). We grew our cultures in a bioreactor (LAMBDA Laboratory Instruments) using minimal media with the composition of yeast nitrogen base (YNB) and supplemented with 2 g/l D-glucose.

Mouse embryonic stem cells (E14 10^{th} passage) were grown as adherent cultures in 10-cm plates with 10 ml DMEM/F12 media supplemented with 10% knockout serum replacement, nonessential amino acids (NEAA supplement), 0.1 mM β-mercapto-ethanol, 1% penicillin and streptomycin, leukemia inhibitory factor (LIF; 1,000 U LIF/ml), and 2*i* (GSK3β and Mek1/2 inhibitors).

Both yeast and mouse embryonic stem cells were lysed by vortexing for 10 min with glass beads in cold polysome lysis buffer (PLB) buffer. The crude extracts obtained from this lysis procedure were clarified by centrifugation. The resulting supernatants were applied to linear 11-ml sucrose gradients (10%–50%) and spun at 35,000 rpm in a Beckman SW41 rotor either for 3 hr (for yeast samples) or for 2.5 hr (for mouse samples). Twelve fractions from each sample were collected using a Gradient Station. More details are available in the Supplemental Information.

ACCESSION NUMBERS

The raw MS data have been deposited in MassIVE (ID: MSV000079280) and in the ProteomeX change (ID: PXD002816). The raw and processed MS data and 3D ribosomal structures color coded according to the RP levels from Figure 3E can be found at http://alum.mit.edu/www/nslavov/Ribosome_Data/

SUPPLEMENTAL INFORMATION

Supplemental Information includes Supplemental Experimental Procedures, Supplemental Discussion, five figures, five tables, one movie, and .pdb files and can be found with this article online at http://dx.doi.org/10.1016/j.celrep.2015.09.056.

AUTHOR CONTRIBUTIONS

Conceptualization, N.S.; Methodology, N.S.; Investigation, N.S., S.S., and B.B.; Writing Original Draft, N.S.; Writing Review and Editing, N.S., S.S., and A.v.O.; Funding Acquisition, A.v.O and N.S.; Resources, A.v.O, E.A., and N.S.; Supervision, N.S.

ACKNOWLEDGMENTS

We thank J. Cate and N. Lintner for helping us color code the variability of RPs on the 3D structure of the yeast ribosomes, P. Vaidyanathan for help with the sucrose gradients, R. Robertson for technical assistance, and M. Jovanovic, Y. Katz, S. Kryazhimskiy, W. Gilbert, P. Vaidyanathan, G. Frenkel, D. Mooijman, J. Alvarez, D. Botstein, and A. Murray for discussions and constructive comments. This work was funded by a grant from the National Institutes of Health to A.v.O. (R01-GM068957) and a SPARC grant to E.A. and N.S.

Received: July 24, 2015
Revised: August 31, 2015
Accepted: September 18, 2015
Published: October 22, 2015

REFERENCES

Arava, Y., Wang, Y., Storey, J.D., Liu, C.L., Brown, P.O., and Herschlag, D. (2003). Genome-wide analysis of mRNA translation profiles in Saccharomyces cerevisiae. Proc. Natl. Acad. Sci. USA *100*, 3889–3894.

Ashe, M.P., De Long, S.K., and Sachs, A.B. (2000). Glucose depletion rapidly inhibits translation initiation in yeast. Mol. Biol. Cell *11*, 833–848.

Ben-Shem, A., Garreau de Loubresse, N., Melnikov, S., Jenner, L., Yusupova, G., and Yusupov, M. (2011). The structure of the eukaryotic ribosome at 3.0 Å resolution. Science *334*, 1524–1529.

Bonven, B., and Gulløv, K. (1979). Peptide chain elongation rate and ribosomal activity in Saccharomyces cerevisiae as a function of the growth rate. Mol. Gen. Genet. *170*, 225–230.

Brauer, M.J., Huttenhower, C., Airoldi, E.M., Rosenstein, R., Matese, J.C., Gresham, D., Boer, V.M., Troyanskaya, O.G., and Botstein, D. (2008). Coordination of growth rate, cell cycle, stress response, and metabolic activity in yeast. Mol. Biol. Cell *19*, 352–367.

Castelli, L.M., Lui, J., Campbell, S.G., Rowe, W., Zeef, L.A., Holmes, L.E., Hoyle, N.P., Bone, J., Selley, J.N., Sims, P.F., and Ashe, M.P. (2011). Glucose depletion inhibits translation initiation via eIF4A loss and subsequent 48S preinitiation complex accumulation, while the pentose phosphate pathway is coordinately up-regulated. Mol. Biol. Cell *22*, 3379–3393.

Castello, A., Fischer, B., Eichelbaum, K., Horos, R., Beckmann, B.M., Strein, C., Davey, N.E., Humphreys, D.T., Preiss, T., Steinmetz, L.M., et al. (2012). Insights into RNA biology from an atlas of mammalian mRNA-binding proteins. Cell *149*, 1393–1406.

Chen, S.S., and Williamson, J.R. (2013). Characterization of the ribosome biogenesis landscape in *E. coli* using quantitative mass spectrometry. J. Mol. Biol. *425*, 767–779.

Dave, B., Granados-Principal, S., Zhu, R., Benz, S., Rabizadeh, S., Soon-Shiong, P., Yu, K.D., Shao, Z., Li, X., Gilcrease, M., et al. (2014) Targeting RPL39 and MLF2 reduces tumor initiation and metastasis in breast cancer by inhibiting nitric oxide synthase signaling. *Proceedings of the National Academy of Sciences* : 201320769

De Bortoli, M., Castellino, R.C., Lu, X.Y., Deyo, J., Sturla, L.M., Adesina, A.M., Perlaky, L., Pomeroy, S.L., Lau, C.C., Man, T.K., et al. (2006). Medulloblastoma outcome is adversely associated with overexpression of EEF1D, RPL30, and RPS20 on the long arm of chromosome 8. BMC Cancer *6*, 223.

De Keersmaecker, K., Atak, Z.K., Li, N., Vicente, C., Patchett, S., Girardi, T., Gianfelici, V., Geerdens, E., Clappier, E., Porcu, M., et al. (2013). Exome sequencing identifies mutation in CNOT3 and ribosomal genes RPL5 and RPL10 in T-cell acute lymphoblastic leukemia. Nat. Genet. *45*, 186–190.

Fabian, M.R., and Sonenberg, N. (2012). The mechanics of miRNA-mediated gene silencing: a look under the hood of miRISC. Nat. Struct. Mol. Biol. *19*, 586–593.

Fortier, S., MacRae, T., Bilodeau, M., Sargeant, T., and Sauvageau, G. (2015). Haploinsufficiency screen highlights two distinct groups of ribosomal protein genes essential for embryonic stem cell fate. Proc. Natl. Acad. Sci. USA *112*, 2127–2132.

Galkin, O., Bentley, A.A., Gupta, S., Compton, B.A., Mazumder, B., Kinzy, T.G., Merrick, W.C., Hatzoglou, M., Pestova, T.V., Hellen, C.U., and Komar, A.A. (2007). Roles of the negatively charged N-terminal extension of *Saccharomyces cerevisiae* ribosomal protein S5 revealed by characterization of a yeast strain containing human ribosomal protein S5. RNA *13*, 2116–2128.

Gilbert, W.V. (2011). Functional specialization of ribosomes? Trends Biochem. Sci. *36*, 127–132.

Goodman, H.M., and Rich, A. (1963). Mechanism of polyribosome action during protein synthesis. Nature *199*, 318–322.

Gupta, V., and Warner, J.R. (2014). Ribosome-omics of the human ribosome. RNA *20*, 1004–1013.

Hardy, S.J. (1975). The stoichiometry of the ribosomal proteins of *Escherichia coli*. Mol. Gen. Genet. *140*, 253–274.

Hendrickson, D.G., Hogan, D.J., McCullough, H.L., Myers, J.W., Herschlag, D., Ferrell, J.E., and Brown, P.O. (2009). Concordant regulation of translation and mRNA abundance for hundreds of targets of a human microRNA. PLoS Biol. *7*, e1000238.

Horos, R., Ijspeert, H., Pospisilova, D., Sendtner, R., Andrieu-Soler, C., Taskesen, E., Nieradka, A., Cmejla, R., Sendtner, M., Touw, I.P., and von Lindern, M. (2012). Ribosomal deficiencies in Diamond-Blackfan anemia impair translation of transcripts essential for differentiation of murine and human erythroblasts. Blood *119*, 262–272.

Jenner, L., Melnikov, S., Garreau de Loubresse, N., Ben-Shem, A., Iskakova, M., Urzhumtsev, A., Meskauskas, A., Dinman, J., Yusupova, G., and Yusupov, M. (2012). Crystal structure of the 80S yeast ribosome. Curr. Opin. Struct. Biol. *22*, 759–767.

Jovanovic, M., Rooney, M.S., Mertins, P., Przybylski, D., Chevrier, N., Satija, R., Rodriguez, E.H., Fields, A.P., Schwartz, S., Raychowdhury, R., et al. (2015). Immunogenetics. Dynamic profiling of the protein life cycle in response to pathogens. Science *347*, 1259038.

Komili, S., Farny, N.G., Roth, F.P., and Silver, P.A. (2007). Functional specificity among ribosomal proteins regulates gene expression. Cell *131*, 557–571.

Kondrashov, N., Pusic, A., Stumpf, C.R., Shimizu, K., Hsieh, A.C., Xue, S., Ishijima, J., Shiroishi, T., and Barna, M. (2011). Ribosome-mediated specificity in Hox mRNA translation and vertebrate tissue patterning. Cell *145*, 383–397.

Kwon, S.C., Yi, H., Eichelbaum, K., Föhr, S., Fischer, B., You, K.T., Castello, A., Krijgsveld, J., Hentze, M.W., and Kim, V.N. (2013). The RNA-binding protein repertoire of embryonic stem cells. Nat. Struct. Mol. Biol. *20*, 1122–1130.

Landry, D.M., Hertz, M.I., and Thompson, S.R. (2009). RPS25 is essential for translation initiation by the Dicistroviridae and hepatitis C viral IRESs. Genes Dev. *23*, 2753–2764.

Lawrence, M.S., Stojanov, P., Mermel, C.H., Robinson, J.T., Garraway, L.A., Golub, T.R., Meyerson, M., Gabriel, S.B., Lander, E.S., and Getz, G. (2014). Discovery and saturation analysis of cancer genes across 21 tumour types. Nature *505*, 495–501.

Lee, A.S.Y., Burdeinick-Kerr, R., and Whelan, S.P. (2013). A ribosome-specialized translation initiation pathway is required for cap-dependent translation of vesicular stomatitis virus mRNAs. Proc. Natl. Acad. Sci. USA *110*, 324–329.

Mauro, V.P., and Edelman, G.M. (2002). The ribosome filter hypothesis. Proc. Natl. Acad. Sci. USA *99*, 12031–12036.

Mazumder, B., Sampath, P., Seshadri, V., Maitra, R.K., DiCorleto, P.E., and Fox, P.L. (2003). Regulated release of L13a from the 60S ribosomal subunit as a mechanism of transcript-specific translational control. Cell *115*, 187–198.

Mulder, A.M., Yoshioka, C., Beck, A.H., Bunner, A.E., Milligan, R.A., Potter, C.S., Carragher, B., and Williamson, J.R. (2010). Visualizing ribosome biogenesis: parallel assembly pathways for the 30S subunit. Science *330*, 673–677.

Noll, H., Staehelin, T., and Wettstein, F. (1963). Ribosomal aggregates engaged in protein synthesis: ergosome breakdown and messenger ribonucleic acid transport. Nature *198*, 632–638.

O'Leary, M.N., Schreiber, K.H., Zhang, Y., Duc, A.C.E., Rao, S., Hale, J.S., Academia, E.C., Shah, S.R., Morton, J.F., Holstein, C.A., et al. (2013). The ribosomal protein Rpl22 controls ribosome composition by directly repressing expression of its own paralog, Rpl22l1. PLoS Genet. *9*, e1003708.

Ori, A., Banterle, N., Iskar, M., Andrés-Pons, A., Escher, C., Khanh Bui, H., Sparks, L., Solis-Mezarino, V., Rinner, O., Bork, P., et al. (2013). Cell type-specific nuclear pores: a case in point for context-dependent stoichiometry of molecular machines. Mol. Syst. Biol. *9*, 648.

Parenteau, J., Durand, M., Morin, G., Gagnon, J., Lucier, J.F., Wellinger, R.J., Chabot, B., and Elela, S.A. (2011). Introns within ribosomal protein genes regulate the production and function of yeast ribosomes. Cell *147*, 320–331.

Qian, W., Ma, D., Xiao, C., Wang, Z., and Zhang, J. (2012). The genomic landscape and evolutionary resolution of antagonistic pleiotropy in yeast. Cell Rep. *2*, 1399–1410.

Ramagopal, S. (1990). Induction of cell-specific ribosomal proteins in aggregation-competent nonmorphogenetic *Dictyostelium discoideum*. Biochem. Cell Biol. *68*, 1281–1287.

Ramagopal, S., and Ennis, H.L. (1981). Regulation of synthesis of cell-specific ribosomal proteins during differentiation of Dictyostelium discoideum. Proc. Natl. Acad. Sci. USA *78*, 3083–3087.

Reschke, M., Clohessy, J.G., Seitzer, N., Goldstein, D.P., Breitkopf, S.B., Schmolze, D.B., Ala, U., Asara, J.M., Beck, A.H., and Pandolfi, P.P. (2013). Characterization and analysis of the composition and dynamics of the mammalian riboproteome. Cell Rep. *4*, 1276–1287.

Sampath, P., Pritchard, D.K., Pabon, L., Reinecke, H., Schwartz, S.M., Morris, D.R., and Murry, C.E. (2008). A hierarchical network controls protein translation during murine embryonic stem cell self-renewal and differentiation. Cell Stem Cell *2*, 448–460.

Shalem, O., Sanjana, N.E., Hartenian, E., Shi, X., Scott, D.A., Mikkelsen, T.S., Heckl, D., Ebert, B.L., Root, D.E., Doench, J.G., and Zhang, F. (2014). Genome-scale CRISPR-Cas9 knockout screening in human cells. Science *343*, 84–87.

Slavov, N., and Botstein, D. (2011). Coupling among growth rate response, metabolic cycle, and cell division cycle in yeast. Mol. Biol. Cell *22*, 1997–2009.

Slavov, N., and Botstein, D. (2013). Decoupling nutrient signaling from growth rate causes aerobic glycolysis and deregulation of cell size and gene expression. Mol. Biol. Cell *24*, 157–168.

Slavov, N., and Dawson, K.A. (2009). Correlation signature of the macroscopic states of the gene regulatory network in cancer. Proc. Natl. Acad. Sci. USA *106*, 4079–4084.

Slavov, N., Airoldi, E.M., van Oudenaarden, A., and Botstein, D. (2012). A conserved cell growth cycle can account for the environmental stress responses of divergent eukaryotes. Mol. Biol. Cell *23*, 1986–1997.

Slavov, N., Budnik, B.A., Schwab, D., Airoldi, E.M., and van Oudenaarden, A. (2014). Constant growth rate can be supported by decreasing energy flux and increasing aerobic glycolysis. Cell Rep. *7*, 705–714.

Vaidyanathan, P.P., Zinshteyn, B., Thompson, M.K., and Gilbert, W.V. (2014). Protein kinase A regulates gene-specific translational adaptation in differentiating yeast. RNA *20*, 912–922.

Wang, X., Chen, C.F., Baker, P.R., Chen, P.L., Kaiser, P., and Huang, L. (2007). Mass spectrometric characterization of the affinity-purified human 26S proteasome complex. Biochemistry *46*, 3553–3565.

Warner, J.R. (1999). The economics of ribosome biosynthesis in yeast. Trends Biochem. Sci. *24*, 437–440.

Warner, J.R., and McIntosh, K.B. (2009). How common are extraribosomal functions of ribosomal proteins? Mol. Cell *34*, 3–11.

Warner, J.R., Knopf, P.M., and Rich, A. (1963). A multiple ribosomal structure in protein synthesis. Proc. Natl. Acad. Sci. USA *49*, 122–129.

Weber, H.J. (1972). Stoichiometric measurements of 30S and 50S ribosomal proteins from Escherichia coli. Mol. Gen. Genet. *119*, 233–248.

Westermann, P., Heumann, W., and Bielka, H. (1976). On the stoichiometry of proteins in the small ribosomal subunit of hepatoma ascites cells. FEBS Lett. *62*, 132–135.

Wettstein, F.O., Staehelin, T., and Noll, H. (1963). Ribosomal aggregate engaged in protein synthesis: characterization of the ergosome. Nature *197*, 430–435.

Wool, I.G. (1996). Extraribosomal functions of ribosomal proteins. Trends Biochem. Sci. *21*, 164–165.

Xue, S., and Barna, M. (2012). Specialized ribosomes: a new frontier in gene regulation and organismal biology. Nat. Rev. Mol. Cell Biol. *13*, 355–369.

Young, R., and Bremer, H. (1976). Polypeptide-chain-elongation rate in Escherichia coli B/r as a function of growth rate. Biochem. J. *160*, 185–194.

Supplemental Information

Differential stoichiometry among core ribosomal proteins

Nikolai Slavov, Stefan Semrau, Edoardo Airoldi, Bogdan A. Budnik, Alexander van Oudenaarden

Correspondence should be addressed to: nslavov@alum.mit.edu

This PDF file includes:

Supplemental Experimental Procedures

Supplemental Discussion

Supplemental Figures S1 to S5

Supplemental References

Captions for Supplemental Tables S1 to S5

Supplemental Experimental Procedures

Cultivation of mouse ESC

Mouse embryonic stem cells (E14 10^{th} passage) were grown as adherent cultures in 10 cm plates with 10 ml DMEM/F12 media supplemented with 10 % knockout serum replacement, nonessential amino acids (NEAA supplement), 0.1 mM β-mercapto-ethanol, 1 % penicillin and streptomycin, leukemia inhibitory factor (LIF; 1,000 U LIF/ml), and $2i$ (GSK3β and Mek 1/2 inhibitors). The growth curve in Figure S1A indicates that the cells grew exponentially at a growth rate of 0.08 per hour, which corresponds to 9 hours doubling time. During the middle of the exponential growth period, the cells were detached from the plate by 2 min incubation with accutase (Millipore) at 37 ^oC. The cells were pelleted by a 2 min centrifugation, and the pellet was frozen immediately in liquid nitrogen.

Cultivation of yeast

All yeast experiments used a prototrophic diploid strain (DBY12007) with a S288c background and wild type HAP1 alleles (Hickman and Winston, 2007). We grew our cultures in a commercial bioreactor (LAMBDA Laboratory Instruments) using minimal media with the composition of yeast nitrogen base (YNB) and supplemented with 2 g/L D-glucose. Before inoculation, the reactor was filled with 2 L of minimal media and warmed up to a working temperature of 30^oC. Then cultures were started by inoculating the media with 100 μl overnight culture from DBY12007. The overnight cultures were prepared by first streaking frozen DBY12007 on YPD plates (YPD; 10 g of Bacto-Yeast extract, 20 g of Bacto-peptone, 20 g of Bacto-agar, and 20 g of glucose in 1000 ml of water) and then growing a single colony in the same minimal media used for the subsequent growth experiment in the bioreactor. The density of the culture used for inoculation was 2×10^7 cells per ml, resulting in an initial density of 10^3 cells/ml for the culture in the reactor. The cultures were grown at 30^oC and continuously stirred to ensure their homogeneity. The culture was aerated with air coming from a compressed gas cylinder (Airgas, AI-B300 breathable air). The incoming flow of air was controlled by a thermal-based mass-flow controller and filtered through a 0.2 μm filter to ensure sterility.

Cell density was measured on Beckman-Coulter Multisizer 4 by counting at least 20,000 single cells (Slavov *et al*, 2011; Slavov and Botstein, 2011). The samples were taken during the first exponential growth phase on glucose carbon source and during the second exponential growth phase on ethanol carbon source (Slavov *et al*, 2014). To take samples without disturbing the cultures, we used a metal tube attached to silicon tubing and a syringe. The metal tube could be inserted in and out of the cultures, and the syringe used to sample the required volume quickly from the homogeneous cultures. The sampling tubing was kept sterile and no culture was left in it after sampling. All samples were immediately filtered, frozen in liquid nitrogen, and processed as described below.

Sucrose gradients and mass spectrometry work flow

Both yeast and mouse embryonic stem cells were lysed by vortexing for 10 min with glass beads in cold PLB (20 mM HEPES-KOH at pH 7.4, 1 % Triton X–100, 2 mM Magnesium Acetate, 100 mM Potassium Acetate, 0.1 mg/ml cycloheximide, and 3 mM DTT). The crude

extracts obtained from this lysis procedure were clarified by centrifugation, and the resulting supernatants were applied to linear 11 ml sucrose gradients ($10\ \% - 50\ \%$) and spun at 35,000 rpm in a Beckman SW41 rotor either for 3 hours (for yeast samples) or for 2.5 hours (for mouse samples). Twelve fractions from each sample were collected using a Gradient Station (BioComp, Cat. # 153-001). The RNA profile across the gradient was measured by Gradient Profiler (BioComp).

Sample preparation

If ribosomes from different sucrose fractions have different stability and/or susceptibility to digestion, incomplete break-down and digestion of ribosomes may influence our quantification. While such differential stability is interesting on its own right, we wanted to clearly separate it from differential protein content, i.e., RP stoichiometry. To achieve that, we used multiple very harsh sample-preparation protocols that powerfully break-down and denature proteins and their complexes. These protocols include: (i) concentrated guanidinium chloride, (ii) 2 % SDS, (iii) SDS gel, and (iv) chloroform acetone precipitation. Samples prepared with these harsh methods resulted in very similar estimates of RP stoichiometry, suggesting that the harsh protocols succeeded in breaking down completely the ribosomes from all fractions. Furthermore, the relative RP levels estimated from MS and western blots are very similar (Figure S3), providing additional evidence that differential stability of ribosomes and/or partial RP digestion are not major factors affecting our data.

The RP levels displayed in the main figures were estimated from sucrose samples broken down by guanidinium chloride: To break-down the ribosomes completely, the analyzed volume from each sucrose fraction was mixed with 4 volumes of 8 M guanidinium chloride and vortexed for at least 10 min at 37 ^oC. This approach is simple to perform and has the advantage of avoiding potential artifacts associated with protein precipitation. For each fraction, the rRNA absorbance measured during sucrose gradient fractions (Figure 1A, Figure 3A, B) corresponded well with the summed precursor-ion-areas of RP peptides, further supporting that ribosomes are broken-down and and their proteins quantified with uniform efficiency across sucrose fractions. The denatured proteins from each sucrose fraction were further processed via the FASP protocol (Wiśniewski *et al*, 2009), and digested with either lys-C or a mixture of trypsin and lys-C (Promega; # V5073). The digestion with the trypsin/lys-C mix resulted in more identified and

quantified peptides, Figure S2. Subsequently each sample was labeled with TMT reagent (Prod # 90061, Thermo Fisher, San Jose, CA) according to the manufacturer's protocol.

Tandem Mass Tags (TMT) mass spectrometry

The labeled set–sample was injected from an auto–sampler into the trapping column (75 μm column ID, 5 cm packed with 5 μm beads on 20 nm pores, from Michrom Bioresources, Inc.) and washed for 15 min; the sample was eluted to analytic column with a gradient from 2 to 32 % of buffer B (0.1 % formic acid in ACN) over 180 min gradient and fed into LTQ Orbitrap Elite (Thermo Fisher, San Jose, CA). The instrument was set to run in TOP 20 MS/MS mode method with dynamic exclusion. After MS1 scan in Orbitrap with 60K resolving power, each ion was submitted to an HCD MS/MS with 15K or 30K resolving power and to CID MS/MS scan subsequently. All quantification data were derived from HCD spectra.

Analysis of mass spectrometry spectra

Mass/charge spectra where analyzed by MaxQuant (Cox and Mann, 2008) (version 1.4.1.2), SEQUEST HT (Eng *et al*, 1994) and Mascot (Cottrell and London, 1999) (Version 2.4.1) run via the Proteome Discover (64bit version 1.4.0.288, Thermo), and standalone Mascot. All searches were run on a Windows server 2008 64 bit operating system with 64 CPU blades and 256 GB of RAM with the following general parameters. Parent ion mass tolerance was set to 20 ppm, mass tolerance for MS/MS ions was set to 0.02 Da for HCD and to 0.6 Da for CID spectra. For all searches, minimal peptide length was specified as 6 amino acids and maximal peptide length as 50 amino acids. The peptide charge state was limited to +7 for searches with MaxQuant. Searches were performed against either the yeast or the mouse uniprot database and common contaminants that were added to the database. Searches had trypsin or lys-C enzyme specificity, allowing 2 missed cleavages. Asn and Gln deamidation and Met oxidation were included as variable modifications in the search parameters.

The search results from all search engines were filtered at 1 % false discovery rate (FDR) on both protein and on peptide levels using the Percolator (Version 2.05 Build Date May 6 2013). The results exported for further analysis included all peptide spectrum matches (PSM) that were assigned to one or more proteins and passed the statistical significance filter. These results

were outputted in the "Evidence File" for MaxQuant and in a peptide–level–results text file for Proteome Discover. The Proteome Discover files are provided as supplementary datasets.

Similar to Schwanhäusser *et al* (2011), we estimated the absolute abundance of proteins by their iBAQ score, since these scores are among the simplest metrics that allow state-of-the-art accuracy of absolute protein quantification. However, the accuracy of all methods for absolute protein quantification, including the iBAQ score, is undermined by extraneous factors, including protein digestion efficiency, peptide ionization efficiency, the presence of co-eluting peptides, and chromatographic aberrations (Peng *et al*, 2012; Lu *et al*, 2006). These extraneous factors can be averaged out in relative protein quantification, i.e., quantifying the same peptide/protein quantified across different fractions or relative to a standard, allowing errors below $10\ \%$ (Ong *et al*, 2002; Blagoev *et al*, 2004; Bantscheff *et al*, 2007; Chen and Williamson, 2013; Altelaar *et al*, 2013). Throughout all main figures, we use this type of relative quantification that is derived from the reporter-ion-intensities (MS2-level); the relative level of each RP is estimated as the median of the relative reporter-ion-intensities of its unique peptides; This relative quantification makes possible much higher accuracy than iBAQ scores do, but does not allow to directly compare the abundances of different proteins. Thus we have chosen to limit our analysis of differential RP stoichiometries to relative-quantification, which is the most quantitatively accurate and unbiased data that current MS methods can provide.

Western blots

The variable RP stoichiometry indicated by our MS data is rather surprising given that for decades the ribosome has been considered the preeminent example of a large RNA–protein complex with a fixed stoichiometry among the constituent core RPs. Thus, we sought to use an independent experimental method, Western blots, to test out findings. While Western blots have lower sensitivity, specificity, and accuracy than MS (Aebersold *et al*, 2013), they also quantify proteins based on an orthogonal method to MS and are thus an excellent method for further testing the variability of the RP stoichiometry.

Because of the lower sensitivity of Western blots, the low–passage E14 ESCs used for the MS measurements did not provide enough protein material for reliable quantification of the polysomes by Western blots. Thus, we used higher passage–number E14 strain that grows

faster and provides enough protein for reliable quantification. We estimated that $5\ \mu l$ of the monosomal fraction and $20\ \mu l$ of the polysomal fraction having $7-10$ ribosomes per mRNAs have about equal amounts of total ribosomal protein, and we validated that by using Rpl32 as the loading control.

Samples of the monosomes and polysomes were run on 16% Tris–Glycine Mini Protein Gels (Lifetechnologies catalog number: EC6498BOX) for 100 min using the instructions of the manufacturer. The proteins were blotted using the semi-dry method and CAPS buffer at pH 11 on PVDF membrane. The RPs were detected with antibodies from Santa Cruz Biotechnology, Inc, Catalog Numbers: sc-25931 for Rpl11, sc-133977 for Rpl32, sc-68873 for Rps14, and sc-133962 for Rps29. After incubation with secondary antibodies and visualization with Super-Signal West Femto Chemiluminescent Substrate (Thermo Scientific, catalog number 34095), all antibodies resulted in a single band at the molecular weight corresponding to the cognate RP. The blots were imaged with AlphaImager System, and the images were quantified with Image Studio Lite, version 4.0. Consistent with the MS data (Figure S3A), the Western Blots data (Figure S3B) indicate that Rps29 and Rps14 are enriched in polysomes, Rpl11 is enriched in monosomes, and Rpl32 does not change (loading control).

Correlation between relative RP levels and fitness

To explore the physiological significance (if any) of the altered RP stoichiometry, we computed the correlation between the fitness of yeast strains with single RP-gene deletions (Qian *et al*, 2012) and the corresponding relative RP levels that we measured (Figure 3). In yeast, 21 pairs of RP-genes encode proteins with identical amino acid sequences within a pair. Since the RPs within these 21 pairs cannot be distinguished by MS, these 21 RPs were excluded from our analysis and not used to compute correlations between RP levels and fitness of RP-delete strains. Furthermore, some RPs that we quantified did not have RP-deletion fitness data and thus could not be included in our correlation analysis.

Supplementary Discussion

Evaluation of factors that may affect the measured RP levels

The estimated RP levels (Figures 1-3) appear to vary significantly between monosomes and polysomes and across the growth conditions. However, this variation might reflect not only stoichiometry changes among the RPs but also other factors and artifacts, such as noise in the MS measurements, a differential distribution of nascent RP polypeptides among monosomes and polysomes, posttranslational modifications (PTMs) of the RPs, and the presence of 90S ribosomal biogenesis particles. In the subsections below we describe our investigation of such potential artifacts. The results of this investigation (Figure S2 and Figure S4), indicate that such potential artifacts are unlikely to contribute significantly to the estimated RP levels (Figures 1-3), suggesting that the stoichiometry among the RPs can change across polyribosomes and physiological conditions in the absence of genetic perturbations.

Noise, coisolation interference and posttranslational modifications (PTMs)

From most RPs, we quantify multiple unique peptides (whose amino acid sequence is found only in one RP and no other protein in the proteome) both in mouse (Figure S2A, C) and in yeast (Figure S2E). In the absence of measurement noise, post-translational modifications (PTMs), or partial peptides (such as nascent poly-peptide chains), the fold-changes of an RP should equal the fold-changes of each unique peptide coming from this RP. Thus the similarity between the fold changes of unique peptides for the same RP, as quantified by the coefficient of variation (CV; the ratio of the standard deviation to the mean), reflects the degree to which the estimated fold–changes for an RP are influenced by post-translational modification, by noise, and by partial protein products. To evaluate the contribution of all these factors to our RP quantification (Figures 1-3), we computed the distributions of CV values for mouse (Figure S2B, D) and for yeast (Figure S2F) for all RPs having multiple quantified unique peptides per RP. These distributions indicate a median CV < 0.25 and thus suggest that PTMs, measurement noise and partial RPs are not dominant factors in the quantification of most RPs. A few fold-changes, however, have larger CVs that might reflect either PTMs or larger noise in the peptide quantification.

Coisolation interference in the quantification of the reporter ions results in underestimation of the fold changes (Bantscheff *et al*, 2007). To reduce the influence of coisolation interference, we filtered out the quantified peptides with large coisolation interference.

Differential distribution of nascent RP polypeptides among monosomes and polysomes

In principle, a differential distribution of nascent RP polypeptides among monosomes and polysomes could contribute to the measured RP changes (Figures 1-3). As discussed above, the low CVs for protein fold-changes quantified from different unique peptides (Figure S2) make this possibility unlikely.

We sought to test the possibility that nascent RP polypeptides contribute to our estimates of RP levels even more directly. First, if nascent RPs contribute significant numbers of peptides to the variation in RP levels in Figures 1-3, the MS1 precursor-area (integrated area under the MS1 spectrum of the precursor ions that reflects peptide abundance) of N-terminal peptides would be higher compared to the MS1 precursor-area of C-terminal peptides. We compared the distributions of MS1 precursor-areas for N-terminal peptides and for C-terminal peptides and found that the two distributions are statistically identical both for yeast and for mouse. This result suggests that nascent RPs do not contribute significantly to the measured changes in the RP stoichiometry. Second, our Western blots for Rpl11, Rps29, Rps14, and Rps32 showed only one band at the expected molecular weight and no lower molecular weight bands that would correspond to growing nascent chains. If present at a significant level in the sucrose fractions, such growing nascent chains should be detected by the antibodies recognizing N-terminal epitops. Indeed, even in the most extreme case when all mRNAs translated by the ribosomes code for RPs, peptides contributed by the nascent chains are less than $1/80 = 1.2\ \%$ of all RP peptides from a digested fraction. Third, some very short RPs, such as Rps29, which is only 56 animo acids long (6.6 kDa), are highly enriched in the mouse fractions having 7-10 ribosomes per mRNA. The mRNA coding for Rps29 cannot physically fit 7-10 ribosomes, and thus the polysomal enrichment of Rps29 and other short RPs cannot possibly be explained by the on-going translation of nascent poly-peptides in the mouse polysomes. More generally, if nascent proteins contribute to the measured variability, our estimates should indicate that longer

RPs are enriched in sucrose fractions having more ribosomes per mRNA since longer mRNA are translated by more ribosomes (Arava *et al*, 2003). We find no such enrichment, suggesting that our measurements are not significantly affected by nascent polypeptide chains. This is particularly clear in the mouse dataset where we quantified sucrose fractions corresponding to 7-10 ribosomes per mRNA.

The 90S ribosomal biogenesis particles

Sucrose gradients separate not only mature ribosomes but also other cellular organelles of comparable size, such as the immature 90S ribosomal biogenesis particles (Granneman and Baserga, 2004; Sykes and Williamson, 2009; Sykes *et al*, 2010; Chen and Williamson, 2013). The 90S particles should have unequal distribution across the gradient, localizing closely to the 80S monosomal peak and decreasing toward the higher sedimentation-velocity region of the polysomes. Thus if the amount of 90S particles is comparable to the amount of ribosomes, 90S particles could contribute significantly to the changes in the RP stoichiometry in Figures 1-3. However, in exponentially growing cells, the 90S ribosomal biogenesis particles are less abundant than the mature ribosomes (Granneman and Baserga, 2004; Sykes and Williamson, 2009; Sykes *et al*, 2010; Chen and Williamson, 2013), and thus unlikely to contribute substantially to the RP peptides that we quantified.

We used our data to evaluate the extent to which immature 90S particles contribute to our estimates of variability among the RPs. Two key factors that determine this contribution are (i) the level and (ii) the sucrose-gradient localization of the 90S. To estimate these two factors, we used the ribosome-biogenesis proteins that are known to be associated with the 90S particle but not with the mature ribosomes (Granneman and Baserga, 2004). These ribosome-biogenesis proteins provide a solid basis for estimating the abundance of the 90S particles relative to the mature ribosomes and the distribution of the 90S particles across the sucrose fractions.

First, we estimated the abundance of the 90S particle relative to the mature ribosomes. From the 180 proteins annotated by the gene ontology (GO:0042254) term "ribosome biogenesis," we have quantified unique peptides for only 14 proteins that are not core structural RPs. These 14 ribosome-biogenesis proteins are represented in our data by very few peptides (9 proteins are represented by a single peptide), which likely reflects the low abundance of these proteins (relative to the RPs) in our sucrose fractions. This conclusion is strongly supported by the

low MS1 precursor-area (integrated area under the MS1 spectrum of the precursor ions) of ribosome-biogenesis peptides compared to the MS1 precursor-area of RP peptides. To obtain a more quantitative estimate for the abundance of 90S relative to the mature ribosomes, we computed and compared the iBAQ scores (Schwanhäusser *et al*, 2011) (a popular measure for absolute protein levels) for the RPs and for the ribosome biogenesis proteins. The iBAQ scores indicate that the detected ribosome biogenesis proteins and thus the 90S particles are about 100 times less abundant than the RPs and thus the mature ribosomes (Figure S4A), consistent with previous observations (Sykes *et al*, 2010).

The mass-spectrometry method used in our study estimates the absolute levels of a peptide from MS1-level integrated-precursor-ion-area, while the relative levels of a peptide/protein across the samples are estimated from MS2-level reporter-ion-intensities. At the MS1-level, the peptides having the same amino-acid sequence from all samples/fractions are quantified as one integrated-precursor-ion-area, and their relative levels across the samples can be estimated only after fragmentation of the precursor ions, i.e., at the MS2 level. Thus the MS1 data that allow direct absolute quantification – and thus comparing the abundances of different proteins – quantifies the total/cumulative amount for each protein in all analyzed fractions. These data were used to estimate iBAQ scores that reflect the absolute levels for both RPs and ribosome biogenesis factors (Figure S4A). We further used the reporter-ion-intensities to quantify the relative levels of all identified proteins. This relative quantification shows that, as expected, ribosome biogenesis factors are enriched in the monosomal fractions. Combining the absolute and the relative quantification, we estimated the absolute levels of RPs and biogenesis factors only in the monosomal fractions (Figure S4B); specifically, the absolute level of a protein in the monosomal fractions equals its iBAQ score times the sum of its reporter-ion-intensities from the monosomal fractions and divided by the sum of its reporter-ion-intensities in the all fractions. These estimates show that even in the monosomal fractions, biogenesis factors are much less abundant than RPs (Figure S4B), and thus ribosome-biogenesis complexes are likely much less abundant than mature ribosomes. The low abundance of ribosome-biogenesis complexes makes them unlikely to contribute significantly to the quantified RP levels. More quantitatively, the data suggest that the proteins derived from the 90S can contribute about $1-3\ \%$ to the RP fold-changes. Since some measured RP fold-changes exceed $100\ \%$, 90S particles are unlikely to be the sole factor causing the differential RP stoichiometry that we measured.

Second, as expected, the 90S ribosome biogenesis peptides are localized to the 80S monosomal fraction and their levels are even lower and constant across the rest of the sucrose gradient. Thus their small contribution is limited to the monosomes and cannot account for the relative RP changes across polysomes that we observed both in yeast and in mouse (Figures 1-3).

Extra-ribosomal complexes of RPs

A few RPs have been reported to perform extra-ribosomal functions (Mazumder *et al*, 2003; Wool, 1996; Warner and McIntosh, 2009). Some of these extra-ribosomal functions of RPs are performed by small complexes containing RPs. For example a Rpl5/Rpl11/5S-rRNA preribosomal complex is involved in the regulation of p53 (Donati *et al*, 2013). Such extra-ribosomal complexes containing RPs are smaller than the mature ribosomes and should not co-sediment in the sucrose fractions that we analyzed (Donati *et al*, 2013; Warner and McIntosh, 2009). This expectation is strongly supported by our MS data: the non ribosomal proteins identified by our MS analysis included translation factors and protein-folding chaperones, but not proteins known to be involved in extra-ribosomal complexes of RPs. Thus, the levels of extra-ribosomal complexes of RPs that may be present in the analyzed sucrose fractions were too low to be detected by and to affect our analysis.

Stoichiometry among RPs

Our data show that while the levels of some RPs increase, the levels of other RPs decrease. These opposite trends indicate that the ratios (stoichiometries) among RPs making up monosomes and polysomes vary. However, our population–average measurements do not indicate the number of distinct ribosomes in each sucrose fraction or the exact RP composition of such distinct ribosomes.

RPs of the small (40S) and the large (60S) subunits are about equally represented among the subset of RPs that increase or decrease across monosomes and polysomes, Figures 1-3. Therefore, preferential enrichment of 40S or 60S in some fractions is very unlikely to contribute to the variation among RPs that we observe.

References

Aebersold R, Burlingame AL, Bradshaw RA (2013) Western blots versus selected reaction monitoring assays: time to turn the tables? *Molecular Cellular Proteomics* **12**: 2381–2382

Altelaar A, Frese CK, Preisinger C, Hennrich ML, Schram AW, Timmers H, Heck AJ, Mohammed S (2013) Benchmarking stable isotope labeling based quantitative proteomics. *Journal of proteomics* **88**: 14–26

Arava Y, Wang Y, Storey JD, Liu CL, Brown PO, Herschlag D (2003) Genome-wide analysis of mRNA translation profiles in *Saccharomyces cerevisiae*. *Proceedings of the National Academy of Sciences* **100**: 3889–3894

Bantscheff M, Schirle M, Sweetman G, Rick J, Kuster B (2007) Quantitative mass spectrometry in proteomics: a critical review. *Analytical and bioanalytical chemistry* **389**: 1017–1031

Blagoev B, Ong SE, Kratchmarova I, Mann M (2004) Temporal analysis of phosphotyrosine-dependent signaling networks by quantitative proteomics. *Nature biotechnology* **22**: 1139–1145

Brauer MJ, Huttenhower C, Airoldi EM, Rosenstein R, Matese JC, Gresham D, Boer VM, Troyanskaya OG, Botstein D (2008) Coordination of Growth Rate, Cell Cycle, Stress Response, and Metabolic Activity in Yeast. *Mol Biol Cell* **19**: 352–367

Chen SS, Williamson JR (2013) Characterization of the Ribosome Biogenesis Landscape in *E. coli* Using Quantitative Mass Spectrometry. *Journal of molecular biology* **425**: 767–779

Cottrell J, London U (1999) Probability-based protein identification by searching sequence databases using mass spectrometry data. *Electrophoresis* **20**: 3551–3567

Cox J, Mann M (2008) MaxQuant enables high peptide identification rates, individualized ppb-range mass accuracies and proteome-wide protein quantification. *Nature biotechnology* **26**: 1367–1372

Donati G, Peddigari S, Mercer CA, Thomas G (2013) 5S ribosomal RNA is an essential component of a nascent ribosomal precursor complex that regulates the Hdm2-p53 checkpoint. *Cell reports* **4**: 87–98

Eng JK, McCormack AL, Yates Iii JR (1994) An approach to correlate tandem mass spectral data of peptides with amino acid sequences in a protein database. *Journal of the American Society for Mass Spectrometry* **5**: 976–989

Granneman S, Baserga SJ (2004) Ribosome biogenesis: of knobs and RNA processing. *Experimental cell research* **296**: 43–50

Hickman M, Winston F (2007) Heme levels switch the function of Hap1 of *Saccharomyces cerevisiae* between transcriptional activator and transcriptional repressor. *Molecular and Cellular Biology* **27**: 7414–7424

Jenner L, Melnikov S, de Loubresse NG, Ben-Shem A, Iskakova M, Urzhumtsev A, Meskauskas A, Dinman J, Yusupova G, Yusupov M (2012) Crystal structure of the 80S yeast ribosome. *Current opinion in structural biology* **22**: 759–767

Lu P, Vogel C, Wang R, Yao X, Marcotte EM (2006) Absolute protein expression profiling estimates the relative contributions of transcriptional and translational regulation. *Nature biotechnology* **25**: 117–124

Mazumder B, Sampath P, Seshadri V, Maitra RK, DiCorleto PE, Fox PL (2003) Regulated release of L13a from the 60S ribosomal subunit as a mechanism of transcript-specific translational control. *Cell* **115**: 187–198

Mulder AM, Yoshioka C, Beck AH, Bunner AE, Milligan RA, Potter CS, Carragher B, Williamson JR (2010) Visualizing ribosome biogenesis: parallel assembly pathways for the 30S subunit. *Science* **330**: 673–677

Ong SE, Blagoev B, Kratchmarova I, Kristensen DB, Steen H, Pandey A, Mann M (2002) Stable isotope labeling by amino acids in cell culture, SILAC, as a simple and accurate approach to expression proteomics. *Molecular cellular proteomics* **1**: 376–386

Peng M, Taouatas N, Cappadona S, van Breukelen B, Mohammed S, Scholten A, Heck AJ (2012) Protease bias in absolute protein quantitation. *Nature methods* **9**: 524–525

Qian W, Ma D, Xiao C, Wang Z, Zhang J (2012) The genomic landscape and evolutionary resolution of antagonistic pleiotropy in yeast. *Cell Reports* **2**: 1399–1410

Schwanhäusser B, Busse D, Li N, Dittmar G, Schuchhardt J, Wolf J, Chen W, Selbach M (2011) Global quantification of mammalian gene expression control. *Nature* **473**: 337–342

Slavov N, Botstein D (2011) Coupling among growth rate response, metabolic cycle, and cell division cycle in yeast. *Molecular Biology of the Cell* **22**: 1997–2009

Slavov N, Budnik B, Schwab D, Airoldi E, van Oudenaarden A (2014) Constant Growth Rate Can Be Supported by Decreasing Energy Flux and Increasing Aerobic Glycolysis. *Cell Reports* **7**: 705 – 714

Slavov N, Macinskas J, Caudy A, Botstein D (2011) Metabolic cycling without cell division cycling in respiring yeast. *Proceedings of the National Academy of Sciences of the United States of America* **108**: 19090–19095

Sykes MT, Shajani Z, Sperling E, Beck AH, Williamson JR (2010) Quantitative Proteomic Analysis of Ribosome Assembly and Turnover *In Vivo*. *Journal of molecular biology* **403**: 331–345

Sykes MT, Williamson JR (2009) A complex assembly landscape for the 30S ribosomal subunit. *Annual review of biophysics* **38**: 197–215

Warner JR, McIntosh KB (2009) How common are extraribosomal functions of ribosomal proteins? *Molecular cell* **34**: 3–11

Wiśniewski J, Zougman A, Nagaraj N, Mann M (2009) Universal sample preparation method for proteome analysis. *Nature methods* **6**: 359–362

Wool IG (1996) Extraribosomal functions of ribosomal proteins. *Trends in biochemical sciences* **21**: 164–165

Supplemental Figures

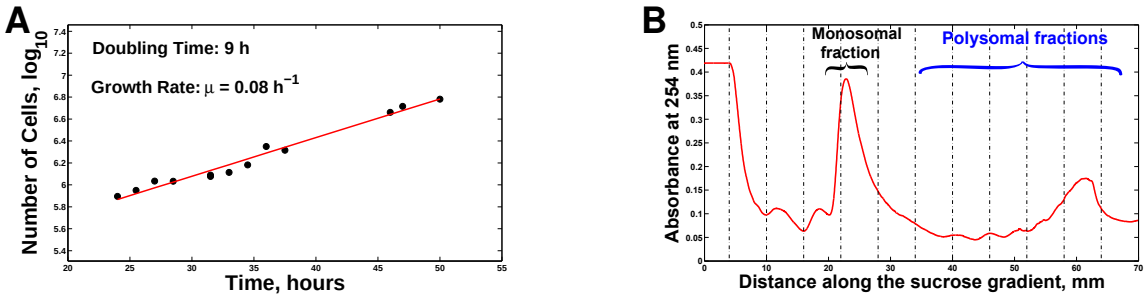

Figure S1. Growth curve of mouse ESCs and a sucrose gradient of neuroprogenitor cells, Related to Figure 1

(**A**) Growth curve of mouse ESCs. At time 0h, 15 ESC cultures were started, and at each time point indicated on the x-xis, one culture was harvested to determine the cell number (y-axis). The cell number is plotted on a log-scale. The data indicate rapid exponential growth at a doubling time of about 9 hours. The ESCs used for our analysis were harvested during the middle of the curve, 35 h after starting the cultures.

(**B**) Sucrose gradient of neuroprogenitor cells (NPCs). The ESCs used in our experiments were differentiated to NPCs, and the ribosomes of the NPCs were fractionated by velocity sedimentation using identical protocol and treatment as those used with ESCs; see the Methods and Extended Appendix for detailed description of the velocity sedimentation.

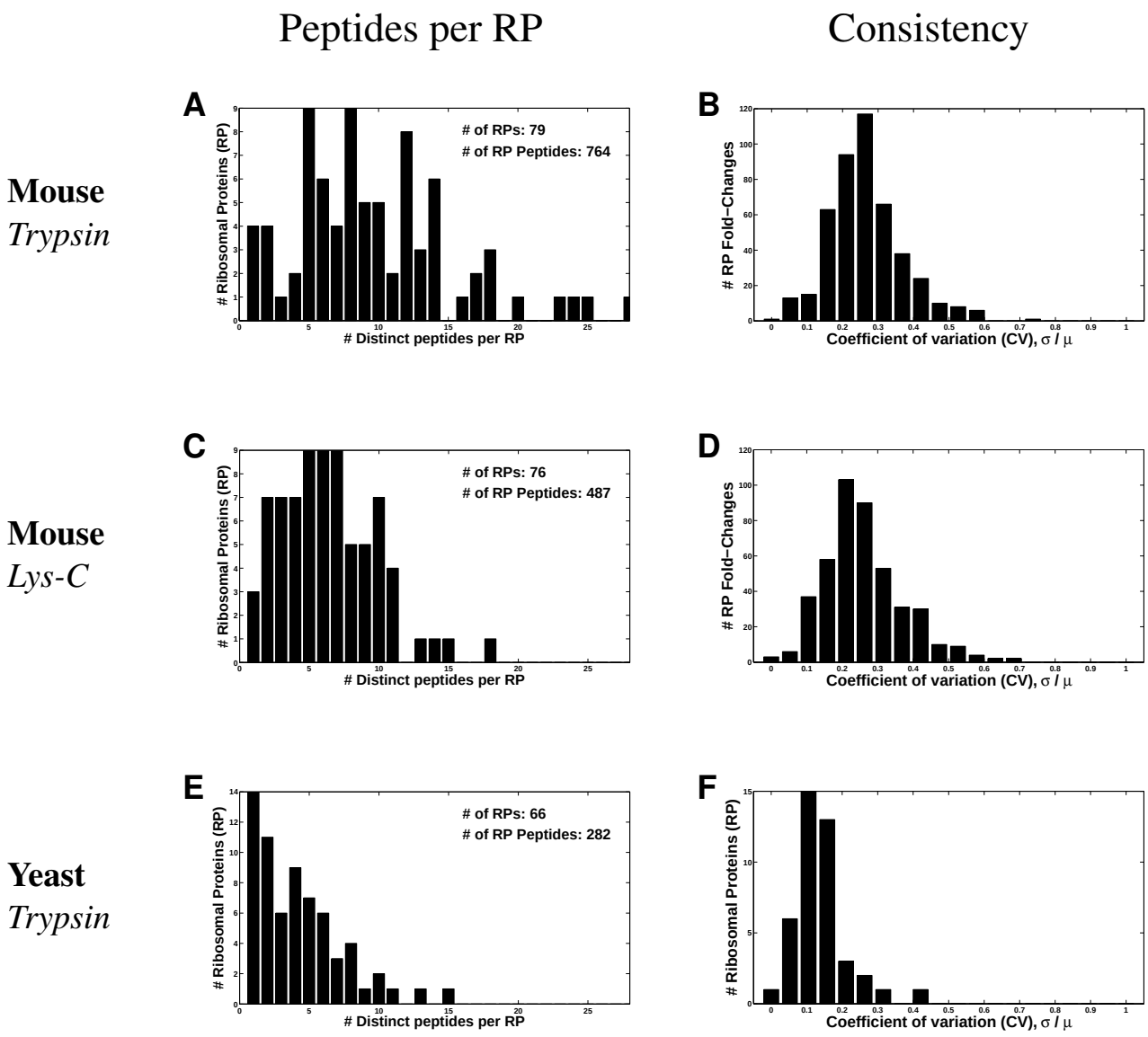

Figure S2. Multiple unique peptides per RP provide consistent fold–change estimates for most RPs, Related to Figures 1-3

(**A**) Number of unique peptides quantified per mouse RP digested by trypsin.

(**B**) Distribution of coefficients of variation (CVs) of the measured fold–changes for mouse RPs digested by trypsin.

(**C**) Number of unique peptides quantified per mouse RP digested by lys-C.

(**D**) Distribution of coefficients of variation (CVs) of the measured fold–changes for mouse RPs digested by lys-C.

(**E**) Number of unique peptides quantified per yeast RP digested by trypsin.

(**F**) Distribution of coefficients of variation (CVs) of the measured fold–changes for yeast RPs digested by trypsin.

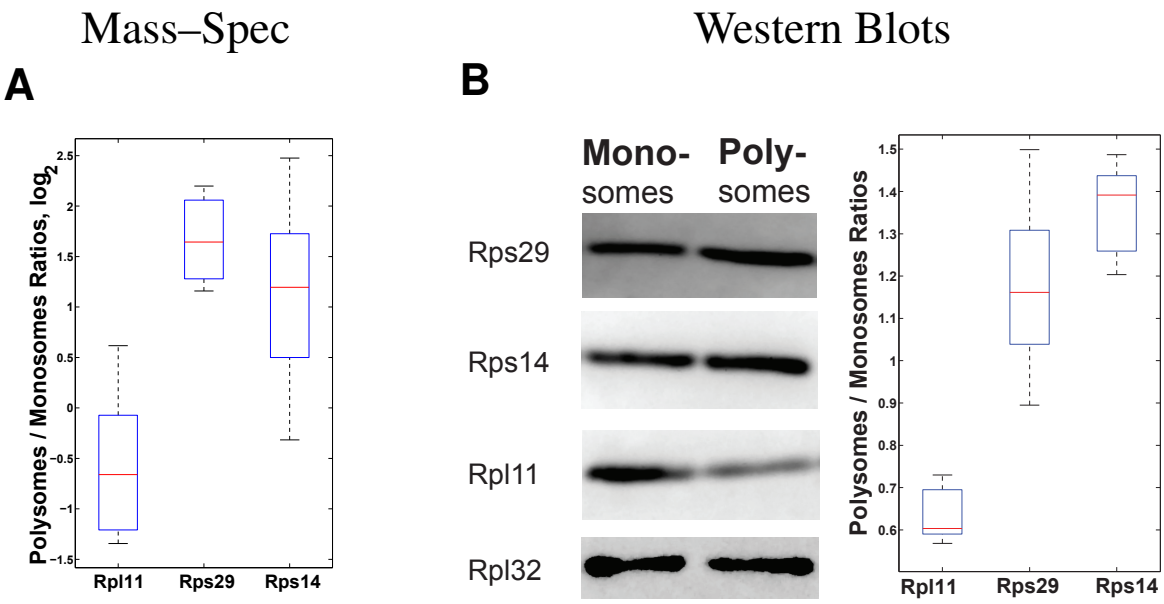

Figure S3. Comparison of relative RP quantification by MS and Western Blots, Related to Figures 1-2.

(**A**) Polysomal enrichment of RPs quantified by MS.

(**B**) Polysomal enrichment of RPs quantified by Western blots. RPs were quantified by Western blots in monosomes and polysomes from high passage–number E14 mouse ESCs. Rpl32 was used as a loading control and the boxplots summarize data from 9 ratios for each quantified RP.

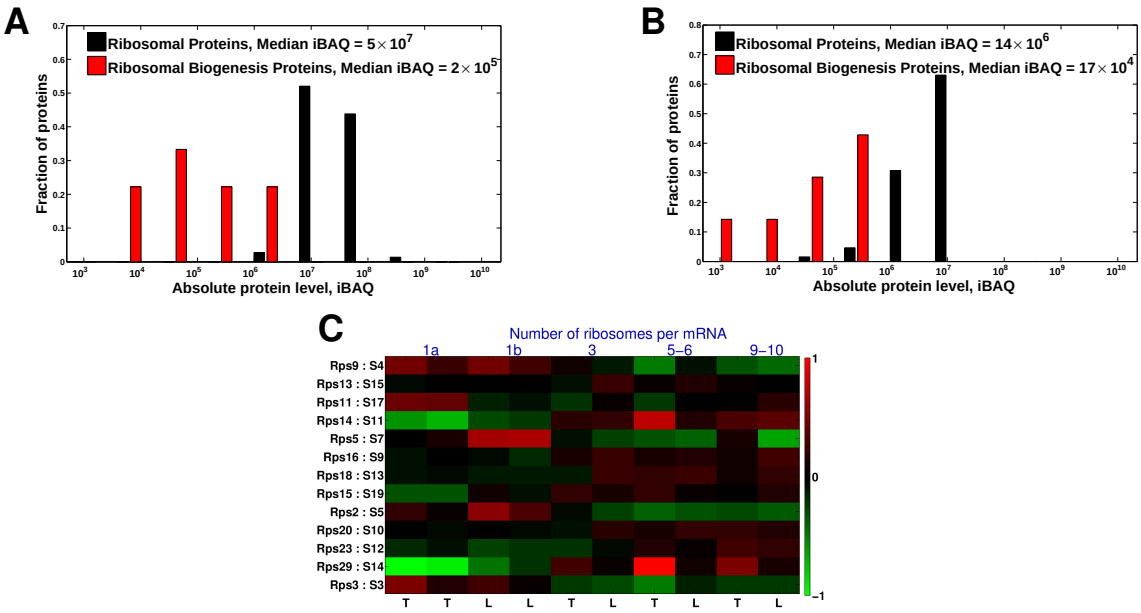

Figure S4. RPs are about 100 fold more abundant that ribosome biogenesis proteins in the sucrose gradients, Related to Figures 1-3

(**A**) Distributions of iBAQ scores for RPs and for ribosome biogenesis proteins. The iBAQ score of a protein estimates its absolute level based on the number of unique peptides for that proteins and their corresponding integrated-precursor-ion-areas. The iBAQ scores are for the total/cumulative amount in all analyzed fractions. The levels of ribosome biogenesis proteins likely reflect the levels of the 90S preribosomal particles in our sucrose gradients.

(**B**) The data from panel (A) was scaled by the reporter-ion intensities to estimate the abundances of RPs and ribosome biogenesis proteins in the monosomal fractions only.

(**C**) The relative levels of mouse RPs are plotted as in Figure 2 but the RPs are arranged in the order in which they are incorporated into the small subunits, as determined by Mulder *et al* (2010); RPs at the top are incorporated first and RPs as the bottom last. Mouse and bacterial RPs were matched based on the correspondence suggested by Jenner *et al* (2012), and the suggested universal ID is listed after the colon.

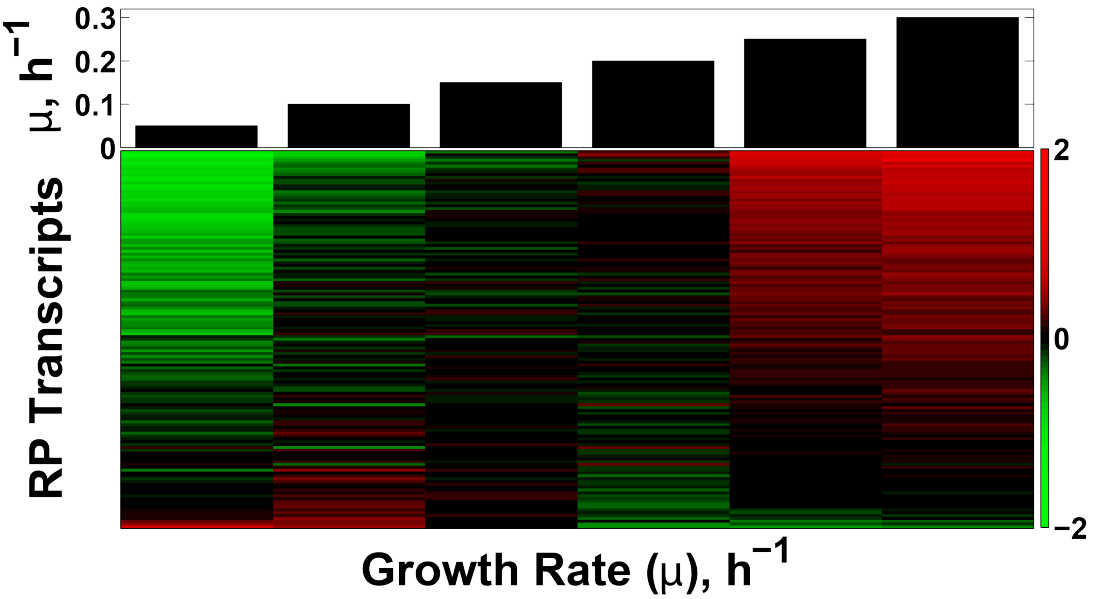

Figure S5. Different RPs have different magnitudes of their growth-rate responses, i.e., transcriptional induction or repression with increasing growth rate, Related to Figure 4. The heatmap displays transcript levels of RPs in yeast cultures growing at steady-state in glucose-limited minimal media at the growth-rates (μ) indicated by the bars on the top. To emphasize the growth-rate trends, the mRNA levels of each RP are displayed on a log_2 scale relative to their mean across all six growth rates. The RPs are sorted by their growth-rate slopes to emphasize the variability of their slopes, from highly positive to negative. All data are from (Slavov and Botstein, 2011; Brauer *et al*, 2008).

Supplemental Tables

Table S1. Normalized protein levels (on a log_2 scale) that are displayed in Figure 2
To facilitate comparison between orthologous RPs, we include the names from the nomenclature suggested by Jenner *et al* (2012).

Table S2. MS data for mouse peptides from the trypsin digestion, Figure 1 and Figure 2
The map of the reporter ions and their corresponding samples from the sucrose gradients is as follows:
TMT-126 – Sucrose fraction corresponding to 1 ribosome per mRNA;
TMT-127 – Sucrose fraction corresponding to 3 ribosome per mRNA;
TMT-129 – Sucrose fraction corresponding to 5-6 ribosome per mRNA;
TMT-130 – Sucrose fraction corresponding to 7-10 ribosome per mRNA;
TMT-131 – Sucrose fraction corresponding to 1 ribosome per mRNA;

Table S3. MS data for mouse peptides from the lys-C digestion, Figure 1 and Figure 2
The map of the reporter ions and their corresponding samples from the sucrose gradients is as follows:
TMT-126 – Sucrose fraction corresponding to 1 ribosome per mRNA;
TMT-127 – Sucrose fraction corresponding to 3 ribosome per mRNA;
TMT-129 – Sucrose fraction corresponding to 5-6 ribosome per mRNA;
TMT-130 – Sucrose fraction corresponding to 7-10 ribosome per mRNA;
TMT-131 – Sucrose fraction corresponding to 1 ribosome per mRNA;

Table S4. Normalized protein levels (on a log_2 scale) that are displayed in Figure 3
To facilitate comparison between orthologous RPs, we include the names from the nomenclature suggested by Jenner *et al* (2012).

Table S5. MS data for yeast peptides from the lys-C digestion, Figure 3
The map of the reporter ions and their corresponding samples from the sucrose gradients is as follows:
TMT-131 – Ethanol: Sucrose fraction corresponding to 1 ribosome per mRNA; Biological replicate 1a
TMT-128N – Ethanol: Sucrose fraction corresponding to 1 ribosome per mRNA; Biological replicate 1b
TMT-128C – Ethanol: Sucrose fraction corresponding to 3 ribosome per mRNA;
TMT-129N – Ethanol: Sucrose fraction corresponding to 4 ribosome per mRNA;
TMT-129C – Glucose: Sucrose fraction corresponding to 1 ribosome per mRNA;
TMT-130N – Glucose: Sucrose fraction corresponding to 3 ribosome per mRNA;
TMT-130C – Glucose: Sucrose fraction corresponding to 4 ribosome per mRNA;